# AI-based Learning of Nonlinear Dynamic System Using IIoT Network with Non-invertible Nonlinear Measurements and Imperfect Channel State Information

| | |
|---|---|
| Journal: | *IEEE Internet of Things Journal* |
| Manuscript ID | IoT-12181-2020 |
| Manuscript Type: | Regular Article |
| Date Submitted by the Author: | 25-Jun-2020 |
| Complete List of Authors: | Cai, Songfu; Hong Kong University of Science and Technology Department of Electronic and Computer Engineering,<br>Lau, Vincent; Hong Kong University of Science and Technology, Dept. of ECE |
| Keywords: | Sensor Signal Processing < Sub-Area 1: Sensors and Devices for IoT, Sensor System Integration < Sub-Area 1: Sensors and Devices for IoT, Resource-Constrained Networks < Sub-Area 2: Communications and Networking for IoT, Sensor and Actuator Networks < Sub-Area 2: Communications and Networking for IoT, Distributed Signal Processing < Sub-Area 3: Services, Applications, and Other Topics for IoT |
| | |

# AI-based Learning of Nonlinear Dynamic System Using IIoT Network with Non-invertible Nonlinear Measurements and Imperfect Channel State Information

Songfu Cai, *Member, IEEE*, Vincent K. N. Lau, *Fellow, IEEE*
Department of Electronic and Computer Engineering
The Hong Kong University of Science and Technology
Clear Water Bay, Kowloon, Hong Kong
Email: {scaiae, eeknlau}@ust.hk

***Abstract*—We consider the artificial intelligence (AI)-based remote state estimation for nonlinear dynamic systems with unknown state dynamics. The nonlinear dynamic plant is monitored by multiple distributed IIoT sensors over a random access wireless network with shared common spectrum. We focus on the remote state estimation algorithm design so as to achieve remote state estimation stability subject to non-invertible nonlinear sensor state observations, imperfect channel state information (CSI) at the remote estimator, and various wireless impairments, such as multi-sensor interference, wireless fading, and additive channel noise. Utilizing a state diffeomorphism, the original system is transformed into a canonical form with a linear rank deficient observation matrix. We propose a novel recurrent neural network (RNN) remote state estimator based on the pole placement design associated with the transformed rank deficient state measurement matrices. We further propose a novel online training algorithm such that the RNN at the remote estimator can not only address the divergence issue over wireless networks but also effectively learn the unknown nonlinear plant dynamics despite rank-deficiency and imperfect CSI. Using the Lyapunov drift analysis approach, we establish closed-form sufficient requirements on the communication resources needed to achieve almost sure stability of both state estimation and RNN online training in the high signal-to-noise ratio (SNR) regime. As a result, our proposed scheme is asymptomatic optimal for large SNR in the sense that both the plant state and the unknown plant nonlinearity can be perfectly recovered at the remote estimator. The proposed scheme is also compared with various baselines and we show that significant performance gains can be achieved.**

***Index Terms*—nonlinear state estimation, recurrent neural networks, imperfect CSI, online training, convergence analysis.**

## I. Introduction

Remote state estimation has received considerable attention in both academia and industry in recent years due to its wide spectrum of applications in environmental monitoring and control, smart grid systems, unmanned aerial vehicles (UAVs), intelligent transportation systems, etc., [1], [2], [3]. A typical remote state estimation system consists of a dynamic plant, a number of wireless IIoT sensors and a remote estimator, as illustrated in Figure 1. Specifically, the IIoT sensors measure the internal states of the plant and transmit the state measurements to the remote estimator over a wireless

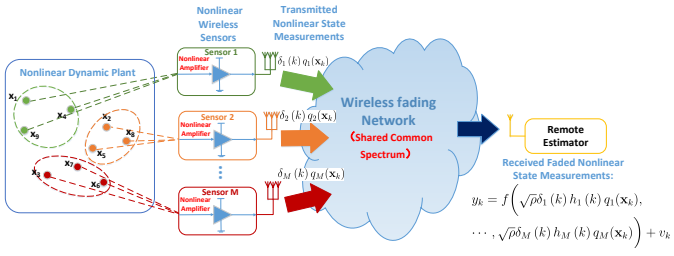


Figure 1. Typical architecture of a remote state estimation system, where all the IIoT sensors share a common spectrum. The $i$-th sensor transmits its nonlinear state measurement $\delta_i(k)\, q_i(\mathbf{x}_k)$ to the remote estimator over a wireless fading channel, where $q_i(\cdot)$ is the nonlinear state measurement function of the $i$-th sensor and $\delta_i(k) \in \{0, 1\}$ is the random access variable of the $i$-th sensor at the $k$-th time slot.

communication network. The remote state estimator generates the real-time plant state estimation based on its received data from the sensors. It is well known that if both the plant dynamics and sensor measurement model are linear, the Kalman filter (KF) is the minimum mean-squared error (MMSE) estimator [4] when the system noises are Gaussian. However, physical dynamic plant and wireless IIoT sensors usually possess various nonlinearities. For example, the kinetic evolutions of the speed and acceleration of a UAV are highly nonlinear [5], and the transfer function of the power amplifier in the transmit datapath of an IIoT sensor is also nonlinear [6]. Such nonlinearities in both plant dynamics and IIoT sensors have been ignored in many existing remote state estimation works [7], [8], [9].

There are some recent works on the remote state estimation of nonlinear dynamics with linear observations. Specifically, in [10] and [11], the authors propose a nonlinear state observer based on the observability of the linear state measurement matrix. In [12], the authors introduce multiplicative Bernoulli noises to the linear state measurements of the sensors to characterize the packet drops in the communication link between each sensor and the remote estimator. The authors propose a dynamic nonlinear state observer adaptive to the packet dropouts, and the stability of the estimator is characterized in

terms of the packet dropout rates. Several other works consider remote estimation of nonlinear dynamics with nonlinear observations. Specifically, in [13], the authors consider the remote state estimation of parallel power systems. They adopt the extended Kalman filter (EKF) to obtain the state estimation based on the nonlinear observations of the voltage magnitudes and phase angles. The dynamic EKF gain matrices are computed based on the linearizations of the nonlinear plant model and the nonlinear observation model. In [14], the authors propose a linear parameter varying (LPV) optimization approach to design the nonlinear observers for Lipschitz nonlinear plant with nonlinear observations. In [15], the authors show that if a nonlinear system is observer error linearizable, then a nonlinear observer canonical form (NOCF) can be utilized for state estimation with nonlinear state measurements. However, in all the aforementioned works [10]-[15], perfect knowledge of plant dynamics is required at the remote estimator, which is usually impractical.

Recently, several other works have considered remote state estimation with unknown nonlinear plant dynamics and linear observations using neural networks. In [16], the authors apply a neural network (NN) to estimate the attitude of a multi-rotor UAV, where only numerical results are provided without theoretical characterization on state estimation performance. In [17] and [18], the authors proposed a nonlinear state estimator, which utilizes an NN to learn the nonlinear plant dynamics, where bounded state estimation mean squared error (MSE) can be achieved under the strictly positive real (SPR) condition and the passivity of the NN activation functions. In [19], the SPR assumption is relaxed at the cost of degraded state estimation performance. In [20], the authors proposed an $e$-modification-based NN online training rule such that passivity of the NN activation functions is not required for state estimation stability. Unfortunately, these standard NN online training algorithms in [16]-[20] are designed for static channels and will diverge over fading channels. In [21] and [22], the authors proposed a KF-based NN online training scheme over fading channels. However, to achieve training convergence, it requires perfect knowledge of the channel state information (CSI) at the remote state estimator, which is impractical. The impact of imperfect CSI on the training convergence is not studied. Moreover, the impacts of nonlinear observations on both the remote state estimation stability and the NN online training convergence have not been considered.

In this paper, we consider the nonlinear remote state estimation over wireless fading channels subject to non-invertible nonlinear sensor measurements and unknown nonlinear plant dynamics. The following summarizes the key contributions of the work.

- **Autonomous Remote State Estimator with Non-Invertible Nonlinear Observations and Imperfect CSI:** Existing NN-based state estimation [16]-[22] cannot be applied to nonlinear observations, and they require perfect CSI at the remote estimator, which is impractical. Utilizing the drift observablility [23], we show that the original system with unknown nonlinear dynamics and nonlinear observations can be transformed into a canonical form with linear equivalent measurement matrices. However, the non-invertible nonlinear measurement will result in rank deficiency of the equivalent measurement matrices, which will introduce penalty to the learning of unknown plant dynamics and result in poor state estimation performance. To address these issues, we propose a novel RNN remote state estimator based on the pole placement design associated with the transformed rank deficient measurement matrices. We show that the proposed RNN state estimator can effectively estimate all the states despite rank deficiency and imperfect CSI.
- **Online Training Algorithm for the RNN and Convergence Analysis:** The existing NN online training algorithms in [16]-[22] diverge over wireless fading channels because the loss functions adopted for NN training do not incorporate the impacts of wireless fadings. Furthermore, these training algorithms are heuristic in nature. To address these issues, we propose a novel online training optimization formulation, where the loss function is constructed based on the pole placement of the linear equivalent measurement matrices. The loss function is designed so that it does not depend on the true plant state and hence, no labeled data will be required to train the RNN. Based on the formulation, we propose a pseudo-gradient descent online training algorithm, which does not require perfect CSI knowledge. We show that the proposed online training converges almost surely to the KKT point of the loss function.
- **Almost Sure State Estimation Stability:** Despite the non-invertible nonlinear observations and the imperfect CSI, the proposed RNN state estimator can achieve stability with a superb MSE under mild conditions. Traditional methods of stability analysis [10]-[12] cannot be applied to obtain closed form stability conditions due to the coupled system state evolutions, where the dynamic evolution of the state estimation error, the RNN training and the fading channel states are tightly coupled together in a very complicated manner. To address the issue, we exploit the *negative Lyapunov drift* to obtain the closed-form sufficient condition for almost sure estimation stability. The closed form condition reveals insights into the impact of the wireless communication resource and the nonlinearity of the plant dynamics as well as the CSI quality on the estimation stability of the system. We show that, in the high SNR regime, the proposed RNN state estimator achieves asymptotically perfect recovery of all the plant states.

*Notation*: Uppercase and lowercase boldface denote matrices and vectors, respectively. The operators $(\cdot)^T$, $(\cdot)^\dagger$, $(\cdot)^H$, $\mathrm{Tr}\,(\cdot)$, and $\mathrm{Re}\,\{\cdot\}$ is the transpose, element-wise conjugate, conjugate transpose, trace, and real part, respectively; $\mathbf{0}_{m\times n}$ denotes $m \times n$ dimensional matrices with all the elements being zero; $||\mathbf{A}||$ denotes the spectrum norm of matrix $\mathbf{A}$; $\mathbf{A}_{ij}$ denotes the element in the $i$-th row and $j$-th column of matrix $\mathbf{A}$; $(\mathbf{A})_i$ denotes the the $i$-th order leading principal submatrix of $\mathbf{A}$; $(\mathbf{A})_{i:j;l:m}$ denotes the $(j-i+1)\times(m-l+1)$ dimensional block submatrix of $\mathbf{A}$ with first element being $\mathbf{A}_{ij}$; $\mathbb{S}_+^K$ denotes the set of $K \times K$ dimensional positive

semidefinite matrices; and $\mathbb{R}^{m\times n}$ ($\mathbb{C}^{m\times n}$) represents the set of $m \times n$ dimensional real (complex) matrices. $\mathcal{C}^{\infty}$ denotes the set of infinitely differentiable functions.

## II. System Model

In this section, we introduce the architecture of the remote state estimation system, nonlinear plant dynamics, nonlinear IIoT sensor model, wireless fading channel model, and the remote state estimation performance metric.

### A. Nonlinear Dynamic Plant Model

A typical remote state estimation system is a spatially distributed system that is comprised of a dynamic plant, multiple distributed wireless sensors, and a remote estimator, as illustrated in Figure 1. The sensors and the remote estimator are geographically separated and are connected over wireless fading channels. We consider a nonlinear discrete-time plant with state dynamics given by:

$$\mathbf{x}_{k+1} = \mathbf{f}\left(\mathbf{x}_k\right), k \geq 0, \tag{1}$$

where $\mathbf{x}_k \in \mathbb{R}^{S\times 1}$ is the plant state process, and $\mathbf{f}\left(\cdot\right) \in \mathcal{C}^{\infty}$: $\mathbb{R}^{S\times 1} \rightarrow \mathbb{R}^{S\times 1}$ is a vector-valued smooth nonlinear state transition function. We assume the nonlinear dynamic plant (1) is stable, i.e., $\left\|\mathbf{f}\left(\cdot\right)\right\| \leq 1$ and $\mathbf{x}_k$ is in a bounded set $\Omega_x$. Additionally, $\mathbf{f}\left(\cdot\right)$ is unknown to the remote state estimator and it has to learn the nonlinear dynamics based on its received observations from the sensors.

As an illustrative example, we consider a single-link flexible-joint manipulator system as shown in Figure 2.

*Example 1: (Single-link Flexible-joint Manipulator)* The single-link flexible-joint manipulator system consists of a rotor, a torsional spring, and a rigid link, as illustrated in Figure 2. At the $k$-th slot, $\theta_l\left(k\right)$, $\omega_l\left(k\right)$ and $\theta_m\left(k\right)$ denotes the link angular position, the link angular velocity, and the rotor torque, respectively. $O$ is the link mass, $l$ is the link length, $K$ is the spring stiffness and $J$ is the rotor inertia.

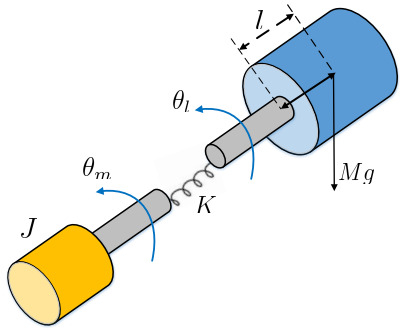


Figure 2. Illustration of a single-link flexible-joint manipulator system.

In Example 1, the system state is $\mathbf{x}_k = \left[\theta_l\left(k\right), \omega_l\left(k\right), \theta_m\left(k\right)\right]^T$ and the evolution of system state $\mathbf{x}_k$ is characterized by $\mathbf{x}_{k+1} = \mathbf{f}\left(\mathbf{x}_k\right)$, where the nonlinear state transition function is given by $\mathbf{f}\left(\mathbf{x}_k\right) = \begin{bmatrix} \omega_l\left(k\right) \\ -\frac{Ogl}{J}\sin\left(\theta_l\left(k\right)\right) + \frac{1}{J}\theta_m\left(k\right) \\ -\omega_l\left(k\right) - \theta_m\left(k\right) \end{bmatrix}$.

### B. Nonlinear Sensor Observation Model

We consider a time-slotted system where a total number of $N$ sensors jointly monitor the nonlinear state process $\mathbf{x}_k$. To enhance the spectral efficiency, all these $N$ sensors share a common radio channel.

Most of the existing state estimation works [7]-[11], [16]-[20], [24]-[27] are only concerned with full rank linear sensor observations models. Specifically, in [24] and [25], the plant state observation of the $i$-th sensor is $\mathbf{C}_i\mathbf{x}_k$, $1 \leq i \leq N$, where the linear state observation matrix $\mathbf{C}_i$ is constrained to be orthogonal, i.e., $\mathbf{C}_i\mathbf{C}_i^T = \mathbf{I}_S$. In [26], the concatenated state observation matrix of the sensors $\left[\mathbf{C}_1^T; \cdots; \mathbf{C}_M^T\right]^T$ is required to be sparse. In [27], $\mathbf{C}_i\mathbf{x}_k$ is required to be non-overlap and the union of $\mathbf{C}_i\mathbf{x}_k$ is the entire system states, i.e., $\bigcup_i \left\{\mathbf{C}_i\mathbf{x}_k\right\} = \mathbf{x}_k$. However, physical wireless sensors usually possess various nonlinearities. For example, the transfer function of each of the power amplifiers in the transmit datapath of the sensors is nonlinear due to the nonlinear power laws of the transistors and vacuum tubes. While previous works [28] and [29] have considered nonlinear observation models, they require the nonlinear map to be invertible, but this is too restrictive. In practice, the nonlinear response may not be invertible. Figure 3 illustrates a power amplifier in the transmit datapath of a wireless sensor with non-invertible nonlinear transfer function $q\left(x_k\right) = \begin{cases} \frac{\sqrt{x_k}}{1+\sqrt{x_k}}, & if\ x_k < 9 \\ \frac{3}{4}, & if\ x_k \geq 9 \end{cases}$. As a result, in this paper, we consider the following nonlinear sensor observation model.

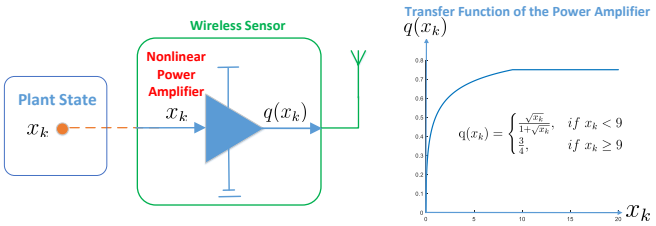


Figure 3. Illustration of the saturation of the non-invertible nonlinear transfer function of a power amplifier in the transmit datapath of a wireless sensor.

*Assumption 1: (Non-Invertible Nonlinear Sensor Observation Model)* The plant state observation of the $i$-th sensor at the $k$-th time slot is given by $q_i\left(\mathbf{x}_k\right) \in \mathbb{R}$, $1 \leq i \leq N$, where $q_i\left(\cdot\right) \in \mathcal{C}^{\infty}$: $\mathbb{R}^{S\times 1} \rightarrow \mathbb{R}$ is a known smooth non-invertible nonlinear function.

Denote the summation of the nonlinear state observations of the sensors as $q\left(\mathbf{x}_k\right) = \sum_{i=1}^{N} q_i\left(\mathbf{x}_k\right)$. We have the following assumption on the observability of $q\left(\cdot\right)$.

*Assumption 2: (Drift-Observability [23])* The nonlinear plant system with state dynamics (1) is drift-observable w.r.t. the nonlinear observations $q\left(\mathbf{x}_k\right)$, i.e., the mapping $\mathbf{\Phi}\left(\cdot\right) : \mathbb{R}^{S\times 1} \rightarrow \mathbb{R}^{S\times 1}$ is a diffeomorphism, where

$$\mathbf{\Phi}\left(\mathbf{x}_k\right) = \begin{bmatrix} q\left(\mathbf{x}_k\right) \\ q\left(\mathbf{f}\left(\mathbf{x}_k\right)\right) \\ \vdots \\ q\left(\mathbf{f}^{(S-1)}\left(\mathbf{x}_k\right)\right) \end{bmatrix}. \tag{2}$$

*Remark 1: (Connection with Observability of Linear Systems)* Note that when both the plant dynamics (1) and the sensor observation model in assumption 1 become linear, i.e., $\mathbf{x}_{k+1} = \mathbf{F}\mathbf{x}_k$ and $q(\mathbf{x}_k) = \mathbf{Q}\mathbf{x}_k$, $\mathbf{\Phi}(\mathbf{x}_k)$ in (2) is reduced to

$$\mathbf{\Phi}\mathbf{x}_k = \begin{bmatrix} \mathbf{Q} \\ \mathbf{QF} \\ \vdots \\ \mathbf{QF}^{S-1} \end{bmatrix} \mathbf{x}_k. \tag{3}$$

Therefore, $\mathbf{\Phi}(\mathbf{x}_k)$ is a diffeomorphism if and only if the observability matrix $\mathbf{\Phi} = [\mathbf{Q}^T; (\mathbf{QF})^T; \ldots, (\mathbf{QF}^{S-1})^T]$ is full column rank. As a result, the drift-observability for nonlinear systems in assumption 2 is backward compatible to the standard notion of observability in linear systems.

### C. Wireless Communication Model

We model the wireless communication channel between the sensors, and the remote estimator as a wireless fading channel. Since all the sensors in the estimation domain share a common radio channel, at the $k$-th time slot, the received signal $y_k \in \mathbb{R}$ at the remote estimator is given by:

$$y_k = \sum_{i=1}^{N} \sqrt{\rho}\delta_i(k) h_i(k) q_i(\mathbf{x}_k) + v_k, \tag{4}$$

where $\sqrt{\rho}$ is the sensor transmission SNR and $\delta_i(k) \in \{0,\ 1\}$ is the $random\ access\ variable$ indicating whether the $i$-th sensor is active to transmit its nonlinear state observation $q_i(\mathbf{x}_k)$ or not, $h_i(k) \in \mathbb{R}$ is the wireless fading channel of the $i$-th sensor, and $v_k \sim \mathcal{N}(0,1)$ is the additive Gaussian channel noise. We have the following assumption on $h_i(k)$.

*Assumption 3: (Wireless Fading Channel Model)* The random fading channel realization $h_i(k)$ between the $i$-th sensor and the remote estimator, $1 \le i \le M$, remains constant within each time slot and is i.i.d. over the slots. Moreover, $h_i(k)$ is i.i.d. Gaussian distributed with zero mean and unit variance.

### D. State Estimation Performance Metric

Denote the history of the received signals at the remote estimator up to the $k$-th time slot as $y_0^k = \{y_0, y_1, \cdots, y_k\}$. The task of the remote estimator is to obtain the state estimation $\hat{\mathbf{x}}_k$ of plant state $\mathbf{x}_k$ based on its received signals $y_0^k$. The state estimation MSE associated with the state estimator $\hat{\mathbf{x}}_k$ is defined as:

$$\mathrm{MSE}(k) = \mathbb{E}\left[ \left\| \mathbf{x}_k - \hat{\mathbf{x}}_k \right\|^2 \middle| y_0^k \right]. \tag{5}$$

The state estimation $\mathrm{MSE}(k)$ is a random variable with randomness induced by the history of the wireless fading channels $\left\{ (h_i)_0^k, 1 \le i \le N \right\}$, sensor random access $\left\{ (\delta_i)_0^k, 1 \le i \le N \right\}$, and the wireless channel noises $\{v_0^k\}$ via the received signals $y_0^k$. We have the following definition on the almost sure state estimation stability.

*Definition 1: (Almost Sure State Estimation Stability)* The remote state estimation MSE is almost surely stable if $\Pr\left( \limsup_{k\to\infty} \mathbb{E}[\mathrm{MSE}(k)] = 0 \right) = 1$, where the expectation $\mathbb{E}[\cdot]$ is taken w.r.t. the randomness of the wireless fading channels, the random access of the sensors, and the wireless channel noises.

In the following sections, we will focus on the NN-based nonlinear remote state estimator design and we will analyze the associated requirements on the communication resource consumption such that almost sure estimation stability can be achieved.

.

## III. Remote State Estimation via RNN

In this section, we first review the existing learning-based remote state estimator. We point out the divergence of the existing NN training algorithm over the wireless fading channels. We further propose a novel RNN-based remote state estimator and the associated RNN online training algorithm, which can effectively address the remote state estimation over fading channels with non-invertible nonlinear observations and imperfect CSI.

### A. Existing Learning-based Remote State Estimator

Due to the unknown nonlinear plant state evolutions, the conventional model-based state estimation approaches, such as the Kalman filter [7]-[9] or extended Kalman filter [13], cannot be applied because the knowledge of the plant model $\mathbf{f}(\cdot)$ is unavailable. To address the state estimation with unknown nonlinear plant dynamics over static channels, a learning-based remote state estimator [16]-[20] is thus proposed. Specifically, the learning-based remote state estimator is locally equipped with a neural network, which is trained to learn the unknown plant dynamics using its received plant state observations $y_k = \sum_{i=1}^{N} \sqrt{\rho} h_i(k) q_i(\mathbf{x}_k)$, from the sensors, where $h_i(k)$ is the static channel gain. The state estimation and NN training of existing learning-based remote state estimator is summarized in the following Algorithm 1.

*Algorithm 1 (Existing Learning-based State Estimator [16]-[20]):*

- *Parameterization of Unknown Plant Dynamics*: Due to the NN's capability of nonlinear function approximation, the unknown plant dynamics (1) can be parameterized by an NN. Specifically, by adding and subtracting $\mathbf{A}\mathbf{x}_k$, the nonlinear plant dynamics (1) become [16]:

$$\mathbf{x}_{k+1} = \mathbf{A}\mathbf{x}_k + \mathbf{g}(\mathbf{x}_k), k \ge 0, \tag{6}$$

where $\mathbf{g}(\mathbf{x}_k) = \mathbf{f}(\mathbf{x}_k) - \mathbf{A}\mathbf{x}_k$, $\mathbf{A} \in \mathbb{R}^{S\times S}$ is a known constant matrix. The unknown nonlinear function $\mathbf{g}(\mathbf{x}_k)$ is parameterized by an NN as follows:

$$\mathbf{g}(\mathbf{x}_k) = \overline{\mathbf{W}}\bar{\varphi}(\mathbf{x}_k) + \bar{\epsilon}(\mathbf{x}_k), \tag{7}$$

where $\overline{\mathbf{W}} \in \mathbb{R}^{S\times M}$ is an unknown weight matrix and is defined as the minimizer of $\|\bar{\epsilon}(\mathbf{x}_k)\|$ for all $\mathbf{x}_k \in \Omega_x$:

$$\overline{\mathbf{W}} = \arg \min_{\overline{\mathbf{W}} \in \mathbb{R}^{S\times M}} \left\{ \sup \left\| \mathbf{g}(\mathbf{x}_k) - \overline{\mathbf{W}}\varphi(\mathbf{x}_k) \right\| \right\}, \mathbf{x}_k \in \Omega_x, \tag{8}$$

$M$ is the number of neurons in the neural network, $\bar{\varphi}(\cdot) : \mathbb{R}^{S\times 1} \to \mathbb{R}^{M\times 1}$ is the transfer function of the neurons and is given by $\bar{\varphi}(\mathbf{x}_k) = [\bar{\varphi}_1(\mathbf{x}_k), \cdots, \bar{\varphi}_M(\mathbf{x}_k)]^T$,

$\bar{\varphi}_i(\mathbf{x}_k) \in \mathbb{R}$ is the sigmoidal function and is given by $\bar{\varphi}_i(\mathbf{x}_k) = 2\left(1+e^{\bar{\theta}_i \mathbf{x}_k}\right)^{-1} - 1$, $\bar{\theta}_i \in \mathbb{R}^{1\times S}$, $1 \le i \le M$, is a known constant vector, and $\bar{\epsilon}(\mathbf{x}_k) \in \mathbb{R}^{S\times 1}$ is the bounded neural network approximation error with $\|\bar{\epsilon}(\mathbf{x}_k)\|_2 \le \bar{\epsilon}_M$.

- *NN Architecture in the Remote Estimator*: The existing learning-based remote state estimator locally utilizes an NN to obtain the approximation $\bar{\mathbf{g}}(\bar{\mathbf{x}}_k)$ of the unknown nonlinear function $\mathbf{g}(\mathbf{x}_k)$ as follows:

$$\bar{\mathbf{g}}(\bar{\mathbf{x}}_k) = \overline{\mathbf{W}}_k \bar{\varphi}(\bar{\mathbf{x}}_k), \tag{9}$$

where $\overline{\mathbf{W}}_k \in \mathbb{R}^{S\times M}$ and $\bar{\mathbf{x}}_k \in \mathbb{R}^{S\times 1}$ is the weight matrix of the NN at the remote estimator, and the estimated state at the $k$-th timeslot, respectively. At the $(k+1)$-th timeslot, based on the received signal $y_k$ and the NN output $\overline{\mathbf{W}}_k\varphi(\bar{\mathbf{x}}_k)$ , the existing learning-based remote state estimator obtains the state estimation $\bar{\mathbf{x}}_{k+1}$ as follows:

$$\bar{\mathbf{x}}_{k+1} = \mathbf{A}\bar{\mathbf{x}}_k + \underbrace{\overline{\mathbf{W}}_k\varphi(\bar{\mathbf{x}}_k)}_{NN} + \mathbf{K}\left(y_k - \sum_{i=1}^{N}\sqrt{\rho}h_i(k)\,q_i(\bar{\mathbf{x}}_k)\right), \tag{10}$$

where $\mathbf{K} \in \mathbb{C}^{S\times 1}$ is a constant estimator gain matrix.

- *Error Function for NN Training*: The existing learning-based remote state estimator adopts the following error function $\overline{V}_k$ for NN training:

$$\overline{V}_k = \frac{1}{2}\|\mathbf{x}_k - \bar{\mathbf{x}}_k\|_F^2. \tag{11}$$

The error function $\overline{V}_k$ is non-negative and achieves its minimum value 0 if and only if $\bar{\mathbf{x}}_k = \mathbf{x}_k$.

- *Online Training Algorithm*: The gradient of the loss function $\overline{V}_k$ is given by

$$\frac{\partial \overline{V}_{k+1}}{\partial \overline{\mathbf{W}}_{k+1}} = -(\mathbf{x}_{k+1} - \bar{\mathbf{x}}_{k+1})\varphi^T(\bar{\mathbf{x}}_k). \tag{12}$$

Since the sensor observation model $q_i(\cdot)$ is non-invertible, the labeled data $\mathbf{x}_k$ is thus unavailable, which results in the unavailability of the true gradient of the loss function $\frac{\partial \overline{V}_{k+1}}{\partial \overline{\mathbf{W}}_{k+1}}$. As a result, the existing learning-based remote state estimator adopts the following modified gradient descent weight update rule to train the NN weight $\overline{\mathbf{W}}_k$:

$$\overline{\mathbf{W}}_{k+1} = \overline{\mathbf{W}}_k + \bar{\eta}\left(y_{k+1} - \sum_{i=1}^{N}\sqrt{\rho}h_i(k+1)\,q_i(\bar{\mathbf{x}}_{k+1})\right)\varphi^T(\bar{\mathbf{x}}_k), \tag{13}$$

where $\bar{\eta} \in \mathbb{R}^{S\times 1}$ is a constant learning rate.

The architecture of the existing learning-based remote state estimator is illustrated in Figure 4. Specifically, at the $(k+1)$-th timeslot, the remote state estimator obtains the error term $\left(y_{k+1} - \sum_{i=1}^{N}\sqrt{\rho}h_i(k)\,q_i(\bar{\mathbf{x}}_{k+1})\right)$ based on its revived signal $y_{k+1}$ and the estimated state $\bar{\mathbf{x}}_{k+1}$, which is then passed to the NN training module for online training of the NN weight $\overline{\mathbf{W}}_k$.

- **Challenge 1: Random Access and Channel Fading:** When we have wireless fading and sensor multiple access, the state measurement matrix becomes random and time-varying, i.e., $h_i(k)$ is a random process with $\mathbb{E}[h_i(k)] = 0$. As a result, the average increment of $\overline{\mathbf{W}}_k$ in the online training (13) of Baseline Algorithm 1 is $\mathbb{E}\left[\left(y_{k+1} - \sum_{i=1}^{N}\sqrt{\rho}h_i(k)\,q_i(\bar{\mathbf{x}}_k)\right)^T\varphi^T(\bar{\mathbf{x}}_k)\right] = 0$. This means that, due to the wireless channel fadings and random access of sensors, there is no information input to the NN training in the average sense.
- **Challenge 2: Non-invertible Nonlinear Observation $q_i(\cdot)$:** The state estimator $\bar{\mathbf{x}}_k$ in (10) may not be stable due to the non-invertible nonlinear observation model $q_i(\cdot)$. This is because there may not exist a constant estimator gain matrix in (10) such that $(\mathbf{A}(\mathbf{x}_k - \bar{\mathbf{x}}_k) \mathbf{K}\sum_{i=1}^{N}\sqrt{\rho}h_i(k)(q_i(\mathbf{x}_k) - q_i(\bar{\mathbf{x}}_k))$ is a contraction mapping w.r.t. the state estimation error $\mathbf{x}_k - \bar{\mathbf{x}}_k$.
- **Challenge 3: Requirement of Perfect Channel State Knowledge:** The error term $\left(y_k - \sum_{i=1}^{N}\sqrt{\rho}h_i(k)\,q_i(\bar{\mathbf{x}}_k)\right)$ serves as the input for both the state estimator $\bar{\mathbf{x}}_k$ in (10) and the online training of $\overline{\mathbf{W}}_k$ in (13). However, the construction of the term $\left(y_k - \sum_{i=1}^{N}\sqrt{\rho}h_i(k)\,q_i(\bar{\mathbf{x}}_k)\right)$ requires perfect knowledge of CSI $\{h_1(k), h_2(k), \ldots, h_N(k)\}$. As a result, imperfect CSI will introduces state dependent noises due to the model mismatch, which may cause divergence of the state estimator $\bar{\mathbf{x}}_k$ and the online training of $\overline{\mathbf{W}}_k$.

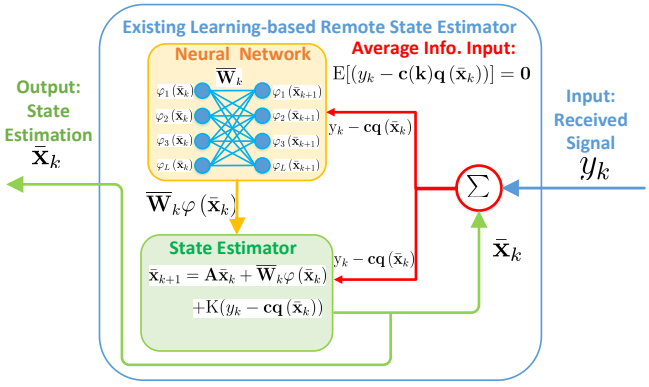


Figure 4. Illustration of the structure of the existing learning-based remote state estimator.

As a result, naively applying the existing learning-based remote state estimator over wireless fading channels with non-invertible nonlinear observations will result in the divergence of state estimation and NN training. This is formally characterized in the following Theorem 1.

*Theorem 1: (Divergence of the Existing Learning-based Remote State Estimator over Wireless Fading Channels with Non-invertible Nonlinear Observations)* The existing learning-based remote state estimator in Baseline Algorithm 1 diverges

over wireless fading channels with non-invertible nonlinear observations.

- *Divergence of NN Training*: the NN weight matrix $\overline{\mathbf{W}}_k$ at the remote estimator always deviates from the unknown true weight $\overline{\mathbf{W}}$ in (7) and $\mathbb{E}\left[\left\|\overline{\mathbf{W}}_k-\overline{\mathbf{W}}\right\|_F^2\right] \geq \left\|\overline{\mathbf{W}}_0-\overline{\mathbf{W}}\right\|_F^2, \forall k \in \mathbb{N}^+$.

  *Proof:* Please see Appendix A. ■

In the next subsections, we shall first establish the equivalence between the nonlinear plant system (1) with non-invertible nonlinear observations and a canonical form with linear equivalent measurement matrices. We then propose a novel RNN remote state estimator based on the pole placement design of the linear equivalent measurement matrices. We shall also propose a novel online training algorithm that can effectively address the divergence of state estimation and NN training over wireless fading channels with non-invertible nonlinear observations.

### B. Equivalent Canonical Form

Non-invertible nonlinear state observations will introduce various challenges to the remote state estimation. For example, the linear-observer-based state estimators [16] and [17], which are designed based on the observability of the linear measurement matrices, cannot work due to the measurement nonlinearity. Although the nonlinear observers developed in [14] and [15] can accommodate nonlinear state measurements, they require the perfect knowledge of the nonlinear plant dynamics, which is impractical. To address this issue, we introduce a smooth nonlinear transformation such that the nonlinear plant dynamics (1) with non-invertible nonlinear observations (4) can be transformed into a canonical form with linear measurement matrices, which is formally characterized by the following Lemma 1.

*Lemma 1: (Equivalent Canonical Form with Linear Measurement Matrices)* Define a smooth nonlinear transformation $\mathbf{\Psi}\left(\cdot\right): \mathbb{R}^{S\times 1} \rightarrow \mathbb{R}^{(N+S)\times 1}$ as:

$$\mathbf{\Psi}\left(\mathbf{x}_k\right) = \left[\begin{array}{c} \mathbf{q}\left(\mathbf{x}_k\right) \\ \mathbf{x}_k \end{array}\right]. \tag{14}$$

Denote the transformed system state $\mathbf{z}_k \in \mathbb{R}^{(N+S)\times 1}$ as $\mathbf{z}_k = \mathbf{\Psi}\left(\mathbf{x}_k\right)$. It follows that:

- *Convertible Mapping*: $\mathbf{\Psi}\left(\cdot\right)$ is invertible and its inverse is given by $\mathbf{\Psi}^{-1}\left(\mathbf{z}_k\right) = \mathbf{\Gamma}\mathbf{z}_k$, where $\mathbf{\Gamma} \in \mathbb{R}^{1\times S}$ is a binary vector and is given by:

$$\mathbf{\Gamma} = [\underbrace{1, \quad \ldots \quad, 1}_{N\ 1s}, \underbrace{0, \quad \ldots \quad, 0}_{S\ 0s}]. \tag{15}$$

- *Equivalent Transformed Dynamic System*: Applying the nonlinear transformation $\mathbf{z}_k = \mathbf{\Psi}\left(\mathbf{x}_k\right)$ to both the nonlinear plant model (1) and the non-invertible nonlinear observation model (4), the original system is equivalent to the following canonical form with linear measurement matrices:

$$\begin{cases} \mathbf{z}_{k+1} & = \mathbf{\Psi}\left(\mathbf{f}\left(\mathbf{\Psi}^{-1}\left(\mathbf{z}_k\right)\right)\right); \\ y_k & = \mathbf{h}_k\mathbf{z}_k + v_k, \end{cases} \tag{16}$$

where $\mathbf{h}_k \in \mathbb{R}^{(N+S)\times 1}$ is the equivalent fading channel vector and is given by:

$$\mathbf{h}_k = \sqrt{\rho}[\delta_1\left(k\right)h_1\left(k\right), \ldots, \delta_N\left(k\right)h_N\left(k\right), \underbrace{0, \quad \ldots \quad, 0}_{S\ 0s}]. \tag{17}$$

*Proof:* Please see Appendix B. ■

It is noted that the construction of the proposed state transformation $\mathbf{\Psi}\left(\cdot\right)$ in (14) does not require the knowledge of the unknown plant dynamics $\mathbf{f}\left(\cdot\right)$. Moreover, the state transformation $\mathbf{\Psi}\left(\cdot\right)$ also preserves the drift-observability of the dynamic plant (1), which is formally summarized in the following Lemma 2.

*Lemma 2: (Drift-Observability of the Transformed Dynamic System)* The transformed dynamic system (16) is drift-observable in the average sense, i.e., the mapping $\widetilde{\mathbf{\Phi}}\left(\cdot\right): \mathbb{R}^{(N+S)\times 1} \rightarrow \mathbb{R}^{S\times 1}$ in (18) is a diffeomorphism.

$$\widetilde{\mathbf{\Phi}}\left(\mathbf{z}_k\right) = \left[\begin{array}{c} \mathbb{E}\left[\left(\sum_{i=1}^N h_i\left(k\right)\right)\mathbf{h}_k\mathbf{z}_k\right] \\ \mathbb{E}\left[\left(\sum_{i=1}^N h_i\left(k\right)\right)\mathbf{h}_k\mathbf{\Psi}\left(\mathbf{f}\left(\mathbf{\Psi}^{-1}\left(\mathbf{z}_k\right)\right)\right)\right] \\ \vdots \\ \mathbb{E}\left[\left(\sum_{i=1}^N h_i\left(k\right)\right)\mathbf{h}_k\left(\mathbf{\Psi}\circ\mathbf{f}\circ\mathbf{\Psi}^{-1}\right)^{S-1}\left(\mathbf{z}_k\right)\right] \end{array}\right]. \tag{18}$$

*Proof:* Please see Appendix B. ■

Although the transformed system (16) has a linear state observation model, the existing learning-based remote state estimator still cannot be applied. This is because, due to the non-invertible nonlinear observation models $\{q_i\left(\cdot\right), 1 \leq i \leq N\}$, the transformed equivalent state measurement matrix is rank deficient, which will induce penalty in the learning of unknown plant dynamics in the existing learning-based remote state estimator. Since the linear equivalent measurement matrix $\mathbf{h}_k$ in (17) is a stochastic process with randomness induced by the random access state of the sensors $\{\delta_1, \delta_2, \cdots, \delta_N\}$ as well as the fading channels $\{h_1, h_2, \cdots, h_N\}$, the existing learning-based remote state estimator requires perfect knowledge of CSI, which is impractical. Moreover, due to the randomness of $\mathbf{h}_k$, the existing learning-based remote state estimator will diverge, as illustrated in Theorem 1. In the next subsection, we shall propose a novel RNN remote state estimator based on the transformed system (16) via pole placement design.

### C. RNN Remote State Estimator with Non-Invertible Nonlinear Observations and Imperfect CSI

Leveraging on the equivalent transformed system dynamics (16), we propose a novel RNN remote state estimator for non-invertible nonlinear observation and imperfect CSI, which is formally characterized in the following Algorithm 2.

*Algorithm 2 (Proposed Pole-Placement-based RNN Estimator):*

- *Parameterization of the Unknown Transformed Plant Dynamics*: Based on the support structure of the linear equivalent measurement matrix $\mathbf{h}_k$ in (17), we construct a

structural invertible constant matrix $\mathbf{U} \in \mathbb{R}^{(N+S)\times(N+S)}$ as follows:

$$\mathbf{U} = \left(\mathbf{\Lambda}\left(\lambda\right)\right)^{-1}\left(\mathbf{I}_{S+N} - \mathrm{diag}\left(\left[\lambda_1^{S+N},\ldots,\lambda_{S+N}^{S+N}\right]\right)\right)\mathbf{\Lambda}\left(\lambda\right)\mathbf{\Pi}, \tag{19}$$

where $\lambda = (\lambda_1, \cdots, \lambda_{N+S})$ is a constant $(N+S)$-pla with $0 < \lambda_i < \lambda_j < 1, \forall 1 \leq i < j \leq (N+S)$; $\mathbf{\Lambda}\left(\lambda\right) \in \mathbb{R}^{(N+S)\times(N+S)}$ is a Vandermonde matrix given by:

$$\mathbf{\Lambda}\left(\lambda\right) = \begin{bmatrix} \lambda_1^{S+N} & \cdots & \lambda_1 & 1 \\ \vdots & \ddots & \vdots & \vdots \\ \lambda_{S+N}^{S+N} & \cdots & \lambda_{S+N} & 1 \end{bmatrix}; \tag{20}$$

and $\mathbf{\Pi} \in \mathbb{R}^{(N+S)\times(N+S)}$ is a binary matrix, which is given by:

$$\mathbf{\Pi} = \begin{bmatrix} \mathbf{0}_{S\times N} & \mathbf{I}_S \\ \mathbf{I}_N & \mathbf{0}_{N\times S} \end{bmatrix}. \tag{21}$$

Since $\mathbf{U}$ is invertible, the unknown transformed nonlinear plant dynamics in (16) can be represented as:

$$\mathbf{\Psi}\left(\mathbf{f}\left(\mathbf{\Psi}^{-1}\left(\mathbf{z}_k\right)\right)\right) = \mathbf{U}\mathbf{U}^{-1}\mathbf{\Psi}\left(\mathbf{f}\left(\mathbf{\Psi}^{-1}\left(\mathbf{z}_k\right)\right)\right). \tag{22}$$

Since $\mathbf{U}^{-1}\mathbf{\Psi}\left(\cdot\right)$, $\mathbf{f}\left(\cdot\right)$ and $\mathbf{\Psi}^{-1}\left(\cdot\right)$ all are smooth functions, the unknown nonlinear function $\mathbf{U}^{-1}\mathbf{\Psi}\left(\mathbf{f}\left(\mathbf{\Psi}^{-1}\left(\mathbf{z}_k\right)\right)\right)$ in (22) is thus smooth in $\mathbf{z}_k$. As a result, $\mathbf{U}^{-1}\mathbf{\Psi}\left(\mathbf{f}\left(\mathbf{\Psi}^{-1}\left(\mathbf{z}_k\right)\right)\right)$ can be parameterized by a neural network as follows:

$$\mathbf{U}^{-1}\mathbf{\Psi}\left(\mathbf{f}\left(\mathbf{\Psi}^{-1}\left(\mathbf{z}_k\right)\right)\right) = \mathbf{W}\varphi\left(\mathbf{z}_k\right) + \epsilon\left(\mathbf{z}_k\right), \tag{23}$$

where $\mathbf{W} \in \mathbb{R}^{S\times M}$ is an unknown weight matrix and is defined as the minimizer of $\|\epsilon\left(\mathbf{z}_k\right)\|$:

$$\mathbf{W} = \arg\min_{\mathbf{W}\in\mathbb{R}^{S\times M}}\left\{\sup\left\|\mathbf{U}^{-1}\mathbf{\Psi}\left(\mathbf{f}\left(\mathbf{\Psi}^{-1}\left(\mathbf{z}_k\right)\right)\right) - \mathbf{W}\varphi\left(\mathbf{z}_k\right)\right\|\right\}, \tag{24}$$

$M$ is the number of neurons in the neural network, $\varphi\left(\cdot\right): \mathbb{R}^{(N+S)\times 1} \to \mathbb{R}^{M\times 1}$ is the transfer function of the neurons and is given by $\varphi\left(\mathbf{z}_k\right) = \left[\varphi_1\left(\mathbf{z}_k\right), \cdots, \varphi_M\left(\mathbf{z}_k\right)\right]^T$, $\varphi_i\left(\mathbf{z}_k\right) \in \mathbb{R}$ is the sigmoidal function and is given by $\varphi_i\left(\mathbf{z}_k\right) = 2\left(1 + e^{\theta_i \mathbf{z}_k}\right)^{-1} - 1$, $\theta_i \in \mathbb{R}^{1\times(N+S)}$, $1 \leq i \leq M$, is a known constant vector, and $\epsilon\left(\mathbf{z}_k\right) \in \mathbb{R}^{(N+S)\times 1}$ is the bounded neural network approximation error with $\|\epsilon\left(\mathbf{z}_k\right)\|_2 \leq \epsilon_M$. Substitute (23) into (22), the unknown transformed nonlinear plant dynamics in (16) thus can be parameterized by an NN as follows:

$$\mathbf{\Psi}\left(\mathbf{f}\left(\mathbf{\Psi}^{-1}\left(\mathbf{z}_k\right)\right)\right) = \mathbf{U}\mathbf{W}\varphi\left(\mathbf{z}_k\right) + \mathbf{U}\epsilon\left(\mathbf{z}_k\right). \tag{25}$$

- *RNN Architecture in the Remote Estimator*: At the $(k+1)$-th timeslot, the proposed remote state estimator first obtains the state estimation $\hat{\mathbf{z}}_k$ of the transformed state $\mathbf{z}_k$ using the following RNN:

$$\underbrace{\hat{\mathbf{z}}_{k+1} = \mathbf{U}\hat{\mathbf{W}}_k\varphi\left(\hat{\mathbf{z}}_k\right)}_{RNN}, \tag{26}$$

where $\hat{\mathbf{W}}_k \in \mathbb{R}^{(S+N)\times M}$ is the RNN weight matrix at the $k$-th timeslot. Based on the estimated transformed state $\hat{\mathbf{z}}_{k+1}$, the remote estimator obtains the state estimation $\hat{\mathbf{x}}_{k+1}$ of the original system state $\mathbf{x}_{k+1}$ as:

$$\hat{\mathbf{x}}_{k+1} = \mathbf{\Psi}^{-1}\left(\hat{\mathbf{z}}_{k+1}\right). \tag{27}$$

- *Imperfect Acquisition of Channel Fading* $\mathbf{h}_k$: At the $k$-th timeslot, besides transmitting the nonlinear state observation $q_i\left(\mathbf{x}_k\right)$, each active sensor also transmits a training pilot symbol $\mathbf{c}_i\mathbf{L}$, where $\mathbf{c}_i \in \mathbb{R}^{1\times(S+N)}$ is a binary vector with the $i$-th element being 1 and all the other elements being 0, $\mathbf{L} \in \mathbb{R}^{(S+N)\times L}$ is a fixed common pilot sequence shared among all the sensors and satisfies $\mathbf{L}\mathbf{L}^T = L\mathbf{I}_{S+N}$, and $L \geq (S+N)$ is the pilot length. The received aggregated training pilot $\mathbf{y}_k^L \in \mathbb{R}^{1\times L}$ at the remote estimator is

$$\mathbf{y}_k^L = \sum_{i=1}^{N}\sqrt{\rho}\delta_i\left(k\right)h_i\left(k\right)\mathbf{c}_i\mathbf{L} + \mathbf{v}_k^L, \tag{28}$$

where $\mathbf{v}_k^L \in \mathbb{R}^{1\times L}$ is the additive Gaussian channel noise and each element of $\mathbf{v}_k^L$ is i.i.d. Gaussian distributed with zero mean and unit variance. The remote estimator obtains the CSI estimation $\hat{\mathbf{h}}_k$ through $\mathbf{y}_k^L$ as follows:

$$\hat{\mathbf{h}}_k = \frac{1}{L}\mathbf{y}_k^L\mathbf{L}^T = \mathbf{h}_k + \frac{1}{L}\mathbf{v}_k^L\mathbf{L}. \tag{29}$$

- *Pole Placement-based Error Function for RNN Training*: The proposed RNN remote state estimator adopts the following error function $V_k$ for RNN training:

$$V_k = \frac{1}{2}\left\|\mathbf{P}^{\frac{1}{2}}\mathbf{U}\left(\mathbf{z}_k - \hat{\mathbf{z}}_k\right)\right\|_F^2, \tag{30}$$

where $\mathbf{P} \in \mathbb{S}_+^{N+S}$ is a positive definite matrix designed based on the pole placement of $\begin{bmatrix} \mathbf{0}_{S\times N} & \mathbf{I}_S \\ \mathbf{I}_N & \mathbf{0}_{N\times S} \end{bmatrix}$ using $\mathbb{E}\left[\mathbf{h}_k^T\mathbf{h}_k\right]$ and is given by:

$$\mathbf{P} = \sum_{i=0}^{\infty}\left(\left(\mathbf{\Pi} - \mathbf{U}\mathbb{E}\left[\mathbf{h}_k^T\mathbf{h}_k\right]\right)^i\right)^T\left(\mathbf{\Pi} - \mathbf{U}\mathbb{E}\left[\mathbf{h}_k^T\mathbf{h}_k\right]\right)^i. \tag{31}$$

- *Online Training with Imperfect CSI*: The gradient of the loss function $V_k$ in (30) is given by:

$$\frac{\partial V_{k+1}}{\partial\hat{\mathbf{W}}_{k+1}} = -\mathbf{U}^T\mathbf{P}\mathbf{U}\left(\mathbf{z}_{k+1} - \hat{\mathbf{z}}_{k+1}\right)^T\varphi^T\left(\hat{\mathbf{z}}_k\right). \tag{32}$$

Since the equivalent measurement matrix $\mathbf{h}_k$ in (17) is rank-deficient and unavailable, the labeled data $\mathbf{z}_{k+1}$ is thus unavailable, which results in the unavailability of the true gradient of the loss function $\frac{\partial V_{k+1}}{\partial\hat{\mathbf{W}}_{k+1}}$. As a result, based on the received data $y_{k+1}$ and the imperfect CSI $\hat{\mathbf{h}}_k$, we propose the following pseudo-gradient descent online training algorithm:

$$\hat{\mathbf{W}}_{k+1} = \hat{\mathbf{W}}_k + \eta\rho^{-1}\mathbf{U}^T\mathbf{P}\mathbf{U}\left(\hat{\mathbf{h}}_k^T\left(y_{k+1} - \hat{\mathbf{h}}_k\hat{\mathbf{z}}_{k+1}\right)\right)^T\varphi^T\left(\hat{\mathbf{z}}_k\right), \tag{33}$$

where $\eta \in \mathbb{R}^+$ is a constant learning rate.

Figure 5 illustrates the architecture of the proposed scheme. As shown, the measured the error term $y_{k+1} - \hat{\mathbf{h}}_k\hat{\mathbf{z}}_{k+1}$ is

weighted by the imperfect CSI $\hat{\mathbf{h}}_k$ and the constant matrix $\mathbf{U}^T\mathbf{P}\mathbf{U}$ before being input to the RNN training module.

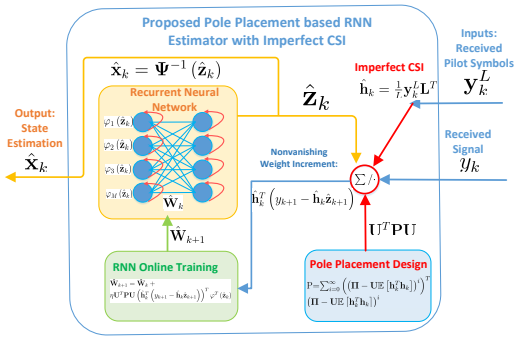


Figure 5. Illustration of the proposed proposed RNN remote state estimator.

*Remark 2: (Pole Placement Structure of the Error Function $V_k$)* Note that the error function $\overline{V}_k$ (11) of the existing online training algorithm 1 is the squared estimation error $\overline{V}_k = \frac{1}{2}\left\|\mathbf{x}_k - \bar{\mathbf{x}}_k\right\|_F^2$ without extra structure. As such, when the measurement matrix is rank deficient, the estimation error of the unmeasurable states is unavailable, which will induce penalty in the training of $\overline{\mathbf{W}}_k$ in (13). In contrast, the proposed error function $V_k$ in (30) has a pole placement structure, which is designed based on the pole placement of $\mathbf{\Pi}$ using matrix $\mathbb{E}\left[\mathbf{h}_k^T\mathbf{h}_k\right]$ and $\mathbf{U}$ in (19). Specifically, due to the structure of $\mathbf{U}$, all the poles of $\left(\mathbf{\Pi} - \mathbf{U}\mathbb{E}\left[\mathbf{h}_k^T\mathbf{h}_k\right]\right)$ are placed to $\lambda = (\lambda_1, \cdots, \lambda_{N+S})$. Since $\lambda_i < 1, \forall 1 \leq i \leq (N+S)$, it follows that the sum of the infinite series $\sum_{i=0}^{\infty}\left(\mathbf{\Pi} - \mathbf{U}\mathbb{E}\left[\mathbf{h}_k^T\mathbf{h}_k\right]\right)^i\left(\left(\mathbf{\Pi} - \mathbf{U}\mathbb{E}\left[\mathbf{h}_k^T\mathbf{h}_k\right]\right)^T\right)^i$ converges. As such, $\|\mathbf{P}\|$ is bounded and the error function $V_k$ is thus well-defined. Moreover, we will show in Section IV that even if the equivalent measurement matrix $\mathbf{h}_k$ is rank deficient, such a pole-placement-structure-induced training algorithm (33) will guarantee a negative Lyapunov drift for the pole placement structured Lyapunov function of $\frac{1}{2}\left\|\mathbf{P}^{\frac{1}{2}}\left(\mathbf{z}_k - \hat{\mathbf{z}}_k\right)\right\|_F^2 + \frac{1}{2}\left\|\mathbf{W} - \hat{\mathbf{W}}_k\right\|_F^2$, which will result in the convergence of both the state estimator $\hat{\mathbf{z}}_k$ and the weight matrix $\hat{\mathbf{W}}_k$.

*Remark 3: (Non-vanishing Pseudo-Gradient over Wireless Channels)* Note that for the existing online training algorithm 1, the expected value of the average increment of the NN weight $\overline{\mathbf{W}}_k$ in (13) vanishes over wireless fading channels, i.e., $\mathbb{E}\left[\left(y_{k+1} - \sum_{i=1}^{N}\sqrt{\rho}h_i(k)\,q_i(\bar{\mathbf{x}}_k)\right)^T\right] = 0$. This means that there is no information input to the NN training in the average sense. In contrast, the average increment of the RNN weight $\hat{\mathbf{W}}_k$ in the proposed RNN online training algorithm (33) will not vanish over wireless networks, i.e., $\mathbb{E}\left[\hat{\mathbf{h}}_k^T\left(y_{k+1} - \hat{\mathbf{h}}_k\hat{\mathbf{z}}_{k+1}\right)\right] \neq \mathbf{0}_{(S+N)\times 1}$. As such, the proposed RNN (26) can still be trained to effectively learn the unknown plant dynamics over wireless fading channels. Moreover, we will show in Section IV-C that, via the proposed online training algorithm (33), the output of the RNN $\mathbf{U}\hat{\mathbf{W}}_k\varphi(\hat{\mathbf{z}}_k)$ will converge almost surely to the unknown nonlinear plant model $\mathbf{\Psi}\left(\mathbf{f}\left(\mathbf{\Psi}^{-1}(\mathbf{z}_k)\right)\right)$ in (16).

In the next section, we shall focus on the stability analysis of the proposed RNN remote state estimator in Algorithm 2 and analyze the sufficient requirement on the communication resources to achieve almost sure estimation stability and online training convergence.

## IV. Stability Analysis

In this section, we analyze the sufficient condition for stability of the proposed RNN remote state estimator and its associated state estimation MSE performance.

### A. Sufficient Condition for Mean-squared Stability

The theory of Lyapunov drift has a long history in the field of stochastic control to analyze the system stability in the fields of both control and communications. As a result, we shall focus on analyzing the stability of the proposed RNN state estimator in Algorithm 2 using Lyapunov techniques [30], [31]. Specifically, denote the state estimator error associated with $\hat{\mathbf{x}}_k$ as $\mathbf{e}_k = \mathbf{x}_k - \hat{\mathbf{x}}_k$, we define a Lyapunov function as follows:

$$\Theta_k = \mathbf{e}_k^T\mathbf{P}\mathbf{e}_k + \frac{1}{\eta}\left\|\mathbf{W} - \hat{\mathbf{W}}_k\right\|_F^2. \tag{34}$$

Note that the $\mathbf{P}$ in (31) is positive semi-definite, the quadratic term $\mathbf{e}_k^T\left(\mathbf{P}_k\right)^{-1}\mathbf{e}_k$ in (34) is thus non-negative. As a result, $\Theta_k$ is non-negative, i.e., $\Theta_k \geq 0, \forall k \in \mathbb{N}^+$. Furthermore, note that $\mathbf{e}_k^T\mathbf{P}\mathbf{e}_k$ achieves its minimum value 0 if and only if $\hat{\mathbf{x}}_k = \mathbf{x}_k$. It follows that $\Theta_k$ reaches its equilibrium $\Theta_k = 0$ if and only if $\hat{\mathbf{x}}_k = \mathbf{x}_k$ and $\hat{\mathbf{W}}_k = \mathbf{W}$. Therefore, $\Theta_k$ is a valid Lyapunov function. The Lyapunov drift associated with $\Theta_k$ is given by

$$\Delta(\Theta_k) = \mathbb{E}\left\{\Theta_{k+1} - \Theta_k \middle| \Theta_k\right\}. \tag{35}$$

Substituting (26), (33) and (34) into (35), we have the following Lemma on the Lyapunov drift $\Delta(\Theta_k)$.

*Lemma 3: (Lyapunov Drift of $\Delta(\Theta_k)$)* The Lyapunov drift $\Delta(\Theta_k)$ is upper bounded as follows:

$$\begin{aligned}\Delta(\Theta_k) \leq \mathbb{E}\Bigg\{ & \left\|\mathbf{P}^{\frac{1}{2}}\mathbf{U}\left(\mathbf{W}\left(\varphi(\mathbf{z}_k) - \varphi(\hat{\mathbf{z}}_k)\right) + \epsilon(\mathbf{z}_k)\right)\right\|_F^2 + \\ & 2\varphi^T(\hat{\mathbf{z}}_k)\left(\mathbf{W} - \hat{\mathbf{W}}_k\right)^T\mathbf{U}^T\mathbf{P}\mathbf{U}\left(\mathbf{W}\left(\varphi(\mathbf{z}_k) - \varphi(\hat{\mathbf{z}}_k)\right) + \epsilon(\mathbf{z}_k)\right) + \\ & \left\|\mathbf{P}^{\frac{1}{2}}\mathbf{U}\left(\mathbf{W} - \hat{\mathbf{W}}_k\right)\varphi(\hat{\mathbf{z}}_k)\right\|_F^2 + 2\varphi^T(\hat{\mathbf{z}}_k)\left(\mathbf{W} - \hat{\mathbf{W}}_k\right)^T\mathbf{U}^T\mathbf{P}\mathbf{U} \\ & \cdot\left(\rho^{-1}\left(\hat{\mathbf{h}}_k^T\mathbf{h}_k + \frac{1}{L}\hat{\mathbf{h}}_k^T\mathbf{v}_k^L\mathbf{L}\right)\hat{\mathbf{e}}_{k+1} - \frac{1}{\rho L}\hat{\mathbf{h}}_k^T\mathbf{v}_k^L\mathbf{L}\mathbf{z}_{k+1}\right) \\ & + \eta\left\|\left(\rho^{-1}\left(\hat{\mathbf{h}}_k^T\mathbf{h}_k + \frac{1}{L}\hat{\mathbf{h}}_k^T\mathbf{v}_k^L\mathbf{L}\right)\hat{\mathbf{e}}_{k+1} - \frac{1}{\rho L}\hat{\mathbf{h}}_k^T\mathbf{v}_k^L\mathbf{L}\mathbf{x}_{k+1}\right)\right\|_F^2 \\ & + \eta\left\|\rho^{-1}\mathbf{P}^{\frac{1}{2}}\mathbf{U}\hat{\mathbf{h}}_k^T v_{k+1}\varphi^T(\hat{\mathbf{z}}_k)\right\|_F^2 - \mathbf{e}_k^T\mathbf{P}\mathbf{e}_k. \end{aligned} \tag{36}$$

*Proof:* Please see Appendix C. ■

The negative Lyapunov drift terms play a central role when applying the Lyapunov drift theory to analyze the stability of dynamic systems. Intuitively, the negative Lyapunov drift is a stabilizing force that pulls the system state back to the equilibrium point [32], [33]. As a result, a sufficient condition for the stability of $\Theta_k$ can be obtained by analyzing the condition for the Lyapunov drift in (36) to be negative. The

closed-form sufficient condition for stability is summarized in the following Theorem 2.

*Theorem 2:* (*Sufficient Condition for Mean-Square Stability of State Estimation and RNN Online Training)* Denote $\tilde{\mathbf{\Pi}} = \mathbf{\Pi} - \mathbf{U}\mathbb{E}\left[\mathbf{h}_k^T\mathbf{h}_k\right]$. If the following condition is satisfied:

$$2\left(\|\mathbf{W}\varphi\| + \frac{1}{\sqrt{\rho L}}\right)\left\|\sum_{i=0}^{\infty}\left(\left(\tilde{\mathbf{\Pi}}\right)^i\right)^T\left(\tilde{\mathbf{\Pi}}\right)^i\right\| + \eta\left\|\sum_{i=0}^{\infty}\left(\left(\tilde{\mathbf{\Pi}}\right)^i\right)^T\left(\tilde{\mathbf{\Pi}}\right)^i\right\|^2 < 1, \tag{37}$$

then the both the state estimation and the RNN online training are stable, i.e., $\limsup_{T\to\infty}\frac{1}{T}\sum_{k=1}^{T}\mathbb{E}\left[\left\|\mathbf{x}_k - \hat{\mathbf{x}}_k\right\|^2\right] < \infty$ and $\limsup_{T\to\infty}\frac{1}{T}\sum_{k=1}^{T}\mathbb{E}\left[\left\|\mathbf{W} - \hat{\mathbf{W}}_k\right\|^2\right] < \infty$.

*Proof:* Please see Appendix D. ∎

The sufficient condition in Theorem 2 delivers some key design insights into the proposed RNN remote state estimation system, which are summarized as follows:

- *Impact of Plant Instability:* The $\|\mathbf{W}\varphi\|$ in (37) characterizes the instability of the nonlinear dynamic plant, and the sufficient condition (37) is difficult to satisfy under large $\|\mathbf{W}\varphi\|$. This means that more communication resource is required for the state estimation and online training stability of more unstable nonlinear dynamic plant.
- *Impact of Imperfect CSI:* Imperfect knowledge of CSI at the remote estimator will introduce a penalty term of $\frac{2}{\sqrt{\rho L}}\|\sum_{i=0}^{\infty}\left(\left(\tilde{\mathbf{\Pi}}\right)^i\right)^T\left(\tilde{\mathbf{\Pi}}\right)^i\|$ in the sufficient condition (37). Note that the CSI estimation error covariance associated with the estimated CSI $\hat{\mathbf{h}}_k$ in (29) is $\mathbb{E}[\left(\mathbf{h}_k - \hat{\mathbf{h}}_k\right)\left(\mathbf{h}_k - \hat{\mathbf{h}}_k\right)^T] = \frac{1}{L}\mathbf{I}_L$. As such, a large channel estimation error, i.e., small $L$, will make the sufficient condition (37) more difficult to satisfy.
- *Impact of Sensor Random Access:* Note that $\tilde{\mathbf{\Pi}} = \left(\mathbf{\Pi} - \mathbf{U}\mathbb{E}\left[\mathbf{h}_k^T\mathbf{h}_k\right]\right)$ characterizes the multiple access of the sensors in the wireless communication network, which battles against the instability of the nonlinear dynamic plant. A large sensor transmission probability $\mathbb{E}\left[\delta_i\left(k\right)\right]$ will lead to small $\|\sum_{i=0}^{\infty}\left(\left(\tilde{\mathbf{\Pi}}\right)^i\right)^T\left(\tilde{\mathbf{\Pi}}\right)^i\|$, and hence the sufficient condition (37) is easier to satisfy. Therefore, more communication resource will result in better state estimation and online training stability performance.

### *B. Almost Sure Stability Analysis*

We are interested in analyzing the achievable state estimation and online training MSE associated with the proposed RNN state estimator in Algorithm 2. This is summarized in the Theorem 3.

*Theorem 3: (MSE of the Proposed RNN State Estimator)* If the sufficient condition (37) in Theorem 2 is satisfied, then the state estimation MSE and online training MSE satisfy:

$$\limsup_{T\to\infty}\frac{1}{T}\sum_{k=1}^{T}\mathbb{E}\left[\left\|\mathbf{x}_k - \hat{\mathbf{x}}_k\right\|^2\right] < \left(2\left\|\sum_{i=0}^{\infty}\left(\left(\tilde{\mathbf{\Pi}}\right)^i\right)^T\left(\tilde{\mathbf{\Pi}}\right)^i\right\| \cdot\left(\epsilon_M^2 + \frac{\alpha}{\rho L}\right) + \frac{\eta\left(S+N\right)}{\rho}\left\|\sum_{i=0}^{\infty}\left(\left(\tilde{\mathbf{\Pi}}\right)^i\right)^T\left(\tilde{\mathbf{\Pi}}\right)^i\right\|^2\right) \cdot\left(1 - 2\left(\|\mathbf{W}\varphi\| + \frac{1}{\sqrt{\rho L}}\right)\left\|\sum_{i=0}^{\infty}\left(\left(\tilde{\mathbf{\Pi}}\right)^i\right)^T\left(\tilde{\mathbf{\Pi}}\right)^i\right\| - \eta\left\|\sum_{i=0}^{\infty}\left(\left(\tilde{\mathbf{\Pi}}\right)^i\right)^T\left(\tilde{\mathbf{\Pi}}\right)^i\right\|^2\right)^{-1}, \tag{38}$$

and

$$\limsup_{T\to\infty}\frac{1}{T}\sum_{k=1}^{T}\mathbb{E}\left[\left\|\mathbf{W}\varphi\left(\mathbf{z}_k\right) - \hat{\mathbf{W}}_k\varphi\left(\hat{\mathbf{z}}_k\right)\right\|^2\right] < 3\epsilon_M^2 + 3\left(1 + \|\mathbf{W}\varphi\|\right) \cdot\left(2\left(\epsilon_M^2 + \frac{\alpha}{\rho L}\right)\left\|\sum_{i=0}^{\infty}\left(\left(\tilde{\mathbf{\Pi}}\right)^i\right)^T\left(\tilde{\mathbf{\Pi}}\right)^i\right\| + \eta\left(S+N\right)\rho^{-1} \cdot\left\|\sum_{i=0}^{\infty}\left(\left(\tilde{\mathbf{\Pi}}\right)^i\right)^T\left(\tilde{\mathbf{\Pi}}\right)^i\right\|^2\right)\left(1 - 2\left(\|\mathbf{W}\varphi\| + \frac{1}{\sqrt{\rho L}}\right) \cdot\left\|\sum_{i=0}^{\infty}\left(\left(\tilde{\mathbf{\Pi}}\right)^i\right)^T\left(\tilde{\mathbf{\Pi}}\right)^i\right\| - \eta\left\|\sum_{i=0}^{\infty}\left(\left(\tilde{\mathbf{\Pi}}\right)^i\right)^T\left(\tilde{\mathbf{\Pi}}\right)^i\right\|^2\right)^{-1}, \tag{39}$$

where $\alpha$ is a bounded constant.

*Proof:* Please see Appendix E. ∎

The state estimation and online training MSE bounds in (38) and (39) reveal the impacts of several key system parameters on the MSE performance of the proposed RNN state estimator, which are summarized below.

- *Sensor Transmit SNR $\rho$:* The sensor transmit SNR $\rho$ related terms in the MSE bounds are $\frac{\alpha}{\rho L}$, $\frac{\eta(S+N)}{\rho}$ and $\frac{1}{\sqrt{\rho L}}$. As a result, the achievable MSE bound in each of (38) and (39) are both decreasing functions of the sensor transmission SNR $\rho$. Therefore, a large sensor transmit SNR $\rho$ is more favorable and will result in a small state estimation and online training MSE.
- *Sensor Pilot Symbol Length $L$:* Similarly, the achievable MSE bound in each of (38) and (39) are both decreasing functions of the sensor pilot symbol length $L$. As such, a large sensor pilot symbol length $L$ is favorable. This is because a large $L$ will induce a small error in the imperfect acquisition of the CSI in (29), which will result in better MSE performance.
- *Number of Neurons $M$ in the RNN:* Note that the NN approximation error term $\epsilon_M$ is of order $\left(\frac{1}{M}\right)^{\frac{1}{S}}$ [16], which decreases as the total number of neurons $M$ in the RNN increases. Therefore, the RNN with a large number of neurons $M$ is favorable for better MSE performance because of its better nonlinear function approximation capability.

As a result, in the high SNR regime, when both the length of the sensor training pilot symbols $L$ and the number of neurons in the RNN $M$ tend to infinity, the MSE of the proposed

RNN remote state estimator is almost surely stable in the sense that the estimated state $\hat{\mathbf{x}}_k$ converges to the true plant state $\mathbf{x}_k$ almost surely, and the weight matrix $\hat{\mathbf{W}}_k$ in the proposed online training algorithm (33) converges almost surely to the true weight matrix $\mathbf{W}$. This is formally summarized in the following Corollary 1.

*Corollary 1: (Almost Sure Convergence of RNN at High SNR)* If the following condition is satisfied:

$$2\left(\left\|\mathbf{\Psi}\circ\mathbf{f}\circ\left(\mathbf{\Psi}^{-1}\right)\right\|\right)\left\|\sum_{i=0}^{\infty}\left(\left(\tilde{\mathbf{\Pi}}\right)^{i}\right)^{T}\left(\tilde{\mathbf{\Pi}}\right)^{i}\right\| + \eta\left\|\sum_{i=0}^{\infty}\left(\left(\tilde{\mathbf{\Pi}}\right)^{i}\right)^{T}\left(\tilde{\mathbf{\Pi}}\right)^{i}\right\|^{2}<1, \tag{40}$$

then in the high SNR regime, the proposed RNN-based remote state estimator in (26) is almost surely stable, i.e.,

$$\Pr\left[\lim_{\rho\to\infty}\lim_{M\to\infty}\lim_{L\to\infty}\limsup_{k\in\mathbb{N}^{+}}\left\|\mathbf{x}_k-\hat{\mathbf{x}}_k\right\|_2^2=0\right]=1. \tag{41}$$

Moreover, via the proposed online training algorithm (33), the proposed RNN in (26) can almost surely recover the transformed unknown plant nonlinearity $\mathbf{\Psi}\left(\mathbf{f}\left(\mathbf{\Psi}^{-1}\left(\cdot\right)\right)\right)$ in (16), i.e.,

$$\Pr\Bigg[\lim_{\rho\to\infty}\lim_{M\to\infty}\lim_{L\to\infty}\limsup_{k\in\mathbb{N}^{+}} \left\|\mathbf{\Psi}\left(\mathbf{f}\left(\mathbf{\Psi}^{-1}\left(\mathbf{z}_k\right)\right)\right)-\mathbf{U}\hat{\mathbf{W}}_k\varphi\left(\hat{\mathbf{z}}_k\right)\right\|^2=0\Bigg]=1. \tag{42}$$

*Proof:* Please see Appendix E. ∎

## V. Numerical Results

In this section, we compare the performance of the proposed RNN-based remote state estimation scheme with the following baselines via numerical simulations.

- **Baseline 1** *(Naive Extended Kalman Filtering [13] with Over-the-Air Aggregation)*: The remote estimator adopts the parameterization of the unknown plant dynamics in (6). Based on the received nonlinear state measurement data $y_k$, the remote state estimator naively adopts the extended Kalman filter in [13] for state estimation without learning the unknown plant nonlinearity $\mathbf{g}\left(\mathbf{x}_k\right)$. Specifically, the state estimation is obtained recursively as $\widetilde{\hat{\mathbf{x}}}_{k+1}=\mathbf{A}\widetilde{\hat{\mathbf{x}}}_k+\mathbf{K}_k\left(y_k-\sum_{i=1}^{N}\sqrt{\rho}h_i\left(k\right)q_i\left(\widetilde{\hat{\mathbf{x}}}_k\right)\right)$, where $\mathbf{K}_k$ is the extended Kalman filtering gain and is given by $\mathbf{K}_k=\mathbf{\Sigma}_k\mathbf{H}_k^T(\mathbf{H}_k\mathbf{\Sigma}_k\mathbf{H}_k^T+\mathbf{I})^{-1}$, $\mathbf{\Sigma}_k$ is obtained recursively as $\mathbf{\Sigma}_{k+1}=\mathbf{A}\left(\mathbf{H}_k^T\mathbf{H}_k+\left(\mathbf{\Sigma}_k\right)^{-1}\right)^{-1}\mathbf{A}$, and $\mathbf{H}_k=\left.\frac{\partial\sum_{i=1}^{N}\sqrt{\rho}h_i(k)q_i(\mathbf{x})}{\partial\mathbf{x}}\right|_{\mathbf{x}=\widetilde{\hat{\mathbf{x}}}_k}$. The multi-access protocol of the sensors is adopted as the over-the-air aggregation MAC scheme [34]. The knowledge of CSI at the remote estimator is assumed to be perfect.
- **Baseline 2** *(Existing Learning-based Remote Estimation with ALOHA and Imperfect CSI)*: The remote estimator adopts the parameterization of the unknown plant dynamics in (6). The remote state estimator adopts the existing learning-based state estimation scheme in (10) for remote state estimation. The remote state estimator adopts the existing NN online training scheme (13) to learn the nonlinear plant dynamics. The sensors randomly access the wireless network according to the ALOHA-based multi-access protocol [35]. The CSI knowledge at the remote estimator is imperfect and is obtained using (29).
- **Baseline 3** *(Existing Learning-based Remote Estimation with Random TDMA and Imperfect CSI)*: The remote estimator adopts the parameterization of the unknown plant dynamics in (6). The remote state estimator adopts the existing learning-based state estimation scheme in (10) for remote state estimation. The remote state estimator adopts the existing NN online training scheme (13) to learn the nonlinear plant dynamics. The sensors randomly access the wireless network according to the random TDMA-based multi-access protocol [36]. The CSI knowledge at the remote estimator is imperfect and is obtained using (29).

We consider a remote state estimation system for which the system parameters are configured as follows: The nonlinear plant state transition function $\mathbf{f}\left(\cdot\right):\mathbb{R}^{6\times1}\rightarrow\mathbb{R}^{6\times1}$ is given by $\mathbf{f}\left(\mathbf{x}\right)=[x_2,-0.5\sin\left(x_1\right)+0.2x_3,-0.7\cos\left(x_2\right)-0.3x_3,0.2x_5,-0.6\cos\left(x_4\right)+0.3x_6,0.3\sin\left(x_5\right)-0.1x_6]^T$; the nonlinear state parameterization matrix $\mathbf{A}$ in Algorithm 1 is chosen as $\mathbf{A}$ =(0.1, -1.2, 0.6, 0.2, 0.7, -0.3; -1, 1.1, 1, 0.8, -0.6, 0.2; -0.5, 0, 0.1, 0.2, 0.7, -1.1; 1, 0.2, 0.6, 0.8, -0.2, 0.9; -0.3, 0.5, -0.8, 1.6, 0.7, -0.1; 0.6, -0.2, 0.6, 0.1, 0.2, 1.8); and the non-invertible nonlinear state observation of the $i$-th sensor at the $k$-th timeslot is $q_i\left(\mathbf{x}_k\right)=x_{\lceil\frac{i}{6}\rceil}+\sin(x_{\lceil\frac{i+1}{6}\rceil})-\cos(x_{\lceil\frac{i+2}{6}\rceil})$.

### A. State Estimation MSE and Online Training Convergence versus Number of Sensors $N$

Figure 6a illustrates the remote state estimation MSE $\mathbb{E}\left[\left\|\mathbf{x}_k-\hat{\mathbf{x}}_k\right\|^2\right]$ versus the number of sensors $N$. It can be observed that, although Baseline 1 can be applied to nonlinear observations, it still has poor state estimation MSE performance because the nonlinearity in the plant dynamics is imprudently ignored in the state estimation. Moreover, as the number of sensors $N$ increases, the state estimation MSE of both Baseline 2 and Baseline 3 becomes extraordinarily large. This is because both Baseline 2 and Baseline 3 are not scalable to a large number of sensors $N$ and cannot accommodate non-invertible nonlinear observations. In contrast, compared with the baseline algorithms, the proposed scheme enjoys substantial state estimation MSE performance gain and has superior scalability to a large number of sensors $N$.

Figure 6b illustrates the online training MSE, i.e., $\mathbb{E}\left[\left\|\overline{\mathbf{W}}\bar{\varphi}\left(\mathbf{x}_k\right)-\overline{\mathbf{W}}_k\bar{\varphi}\left(\bar{\mathbf{x}}_k\right)\right\|^2\right]$ for Baseline 2 and 3, and $\mathbb{E}\left[\left\|\mathbf{W}\varphi\left(\mathbf{z}_k\right)-\hat{\mathbf{W}}_k\varphi\left(\hat{\mathbf{z}}_k\right)\right\|^2\right]$ for the proposed scheme, versus the number of sensors $N$. It can be observed that, as the number of sensors $N$ increases, the NN training MSE of both Baseline Algorithm 2 and Baseline Algorithm 3 becomes extraordinarily large. This is because the existing NN training algorithm adopted both Baseline Algorithm 2 and Baseline

Algorithm 3 diverges over wireless fading channels and cannot accommodate non-invertible nonlinear observations. In contrast, the proposed online training scheme has significant training MSE performance gain and superior scalability to a large number of sensors $N$.

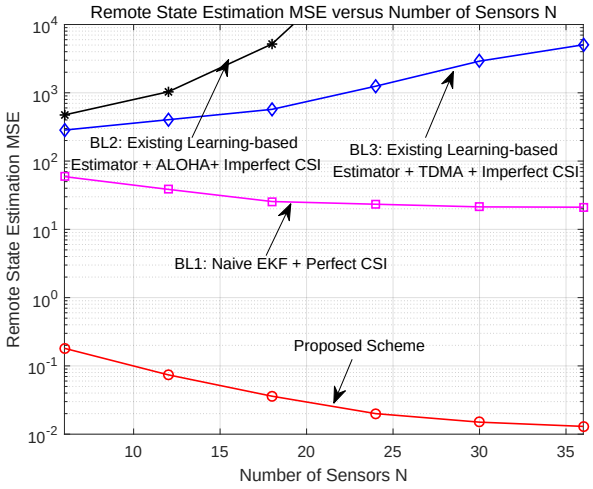


(a) State estimation MSE versus the number of sensors $N$.

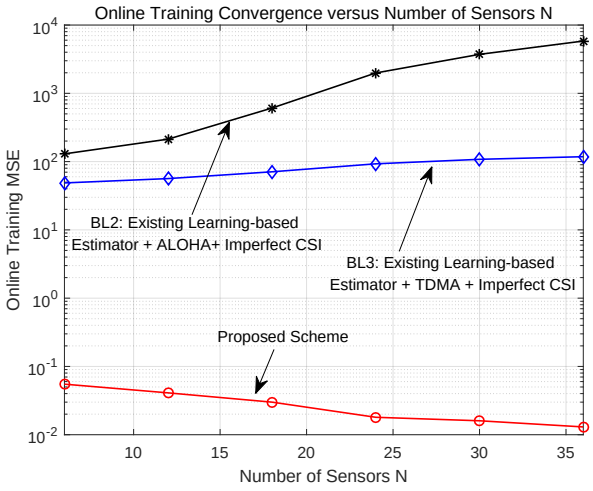


(b) Online training MSE versus the number of sensors $N$.

Figure 6. Illustration of state estimation and online training performance versus the number of sensors $N$. The system parameters are configured as follows: the online training parameter $\bar{\eta} = 0.045\mathbf{I}_{6\times 1}$, $\eta = 0.045$, the sensor transmission probability $\mathbb{E}\left[\delta_i\left(k\right)\right] = 0.2$, the sensor transmission SNR $\rho = 10$ dB, the sensor training pilot length $L = 36$, and the number of neurons in the NN of Baseline 2 and 3 and the number of neurons in the RNN of the proposed scheme is $M = 6$.

### *B. State Estimation MSE and Online Training Convergence versus Sensor Transmission SNR $\rho$*

Figure 7a and 7b illustrates the remote state estimation MSE and online training MSE, respectively, versus the sensor transmission SNR $\rho$. It can be observed that, with the increase of the sensor transmission SNR $\rho$, both the state estimation and online training MSE of all the baselines are still prohibitively large. In contrast, for the proposed scheme, both the state estimation and online training MSE decrease significantly as the sensor transmission SNR $\rho$ increases, which results in substantial MSE performance gain compared with the baseline algorithms.

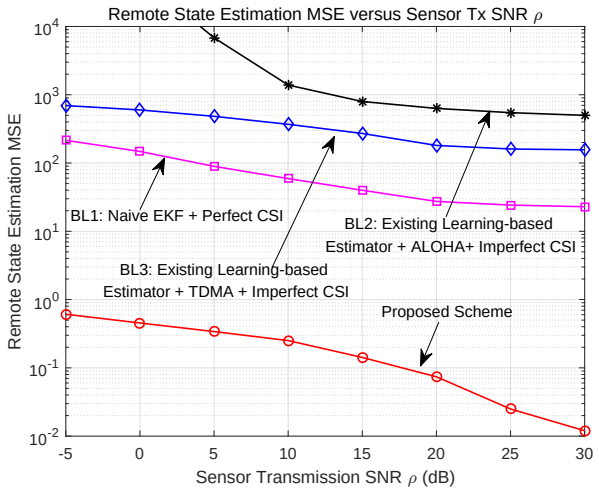


(a) State estimation MSE versus the sensor transmission SNR $\rho$.

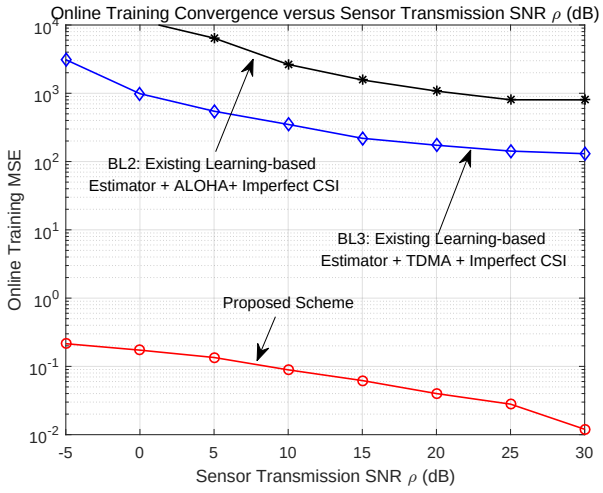


(b) Online training MSE versus the sensor transmission SNR $\rho$.

Figure 7. Illustration of state estimation and online training performance versus sensor transmission SNR $\rho$. The system parameters are configured as follows: the online training parameter $\bar{\eta} = 0.045\mathbf{I}_{6\times 1}$, $\eta = 0.045$, the sensor transmission probability $\mathbb{E}\left[\delta_i\left(k\right)\right] = 0.2$, the number of sensors $N = 6$, the sensor training pilot length $L = 36$, and the number of neurons in the NN of Baseline 2 and 3 and the number of neurons in the RNN of the proposed scheme is $M = 6$.

### *C. State Estimation MSE and Online Training Convergence versus Sensor Training Pilot Length L*

Figure 8a and 8b illustrates the remote state estimation MSE and online training MSE, respectively, versus the sensor training pilot length $L$. Although the CSI estimation quality improves as the training pilot length $L$ increases, the state estimation and online training MSE of Baseline 2 and Baseline 3 are still prohibitively large because of the divergence of estimation and training over wireless fading channels and the incapability to handle non-invertible nonlinear state observations. In contrast, the proposed scheme enjoys substantial

MSE performance gain compared with the baseline algorithms. Specifically, leveraging the better CSI estimation quality at the remote estimator, both the state estimation and online training MSE of the proposed scheme decrease dramatically as the sensor training pilot length $L$ increases.

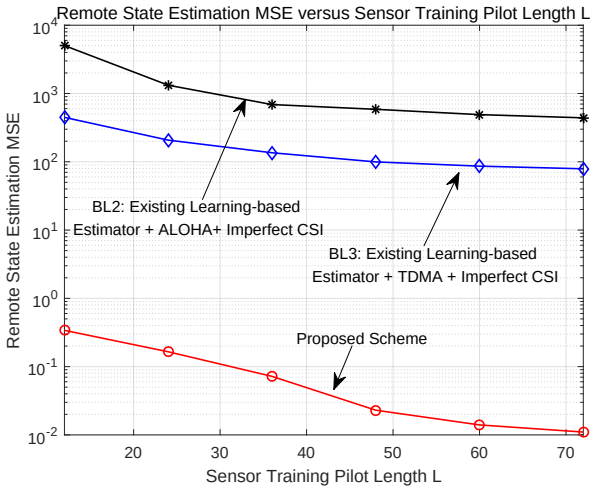


(a) State estimation MSE versus the sensor training pilot length $L$.

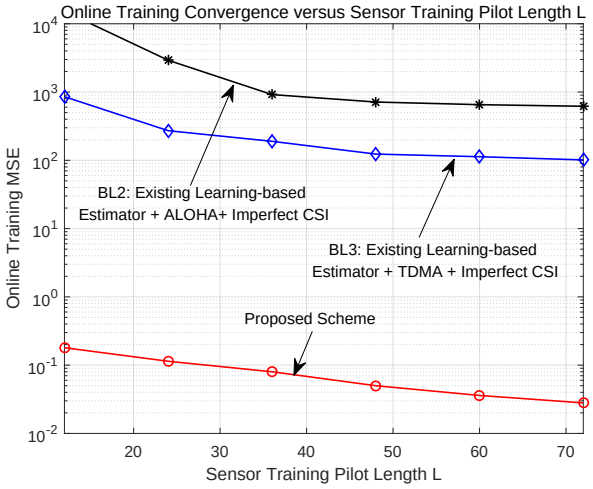


(b) Online training MSE versus the sensor training pilot length $L$.

Figure 8. Illustration of state estimation and online training performance versus sensor training pilot length $L$. The system parameters are configured as follows: the online training parameter $\bar{\eta} = 0.045\mathbf{I}_{6\times 1}$, $\eta = 0.045$, the sensor transmission probability $\mathbb{E}\left[\delta_i\left(k\right)\right] = 0.2$, the number of sensors $N = 6$, the sensor transmission SNR $\rho = 10$ dB, and the number of neurons in the NN of Baseline 2 and 3 and the number of neurons in the RNN of the proposed scheme is $M = 6$.

### *D. State Estimation MSE and Online Training Convergence versus Neurons $M$*

Figure 9a and 9b illustrates the remote state estimation MSE and online training MSE, respectively, versus the number of neurons $M$. It is noted that as the number of neurons $M$ increases, the neural network approximation error will decrease, which means that the neural network can approximate the unknown nonlinear plant dynamics more precisely. However, the state estimation and online training MSE of Baseline 2 and Baseline 3 are still very large due to the divergence of the existing NN-based state estimator and the non-invertible nonlinear observations. On the contrary, due to the enhanced nonlinear function approximation precision, both the state estimation and online training MSE of the proposed scheme decrease significantly as as the number of neurons $M$ increases.

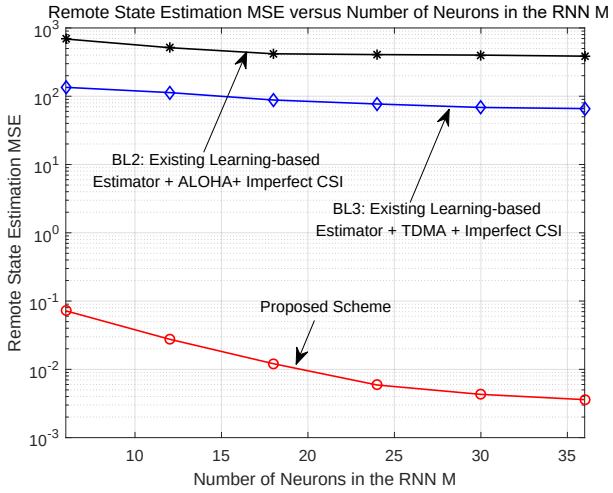


(a) State estimation MSE versus the number of neurons $M$.

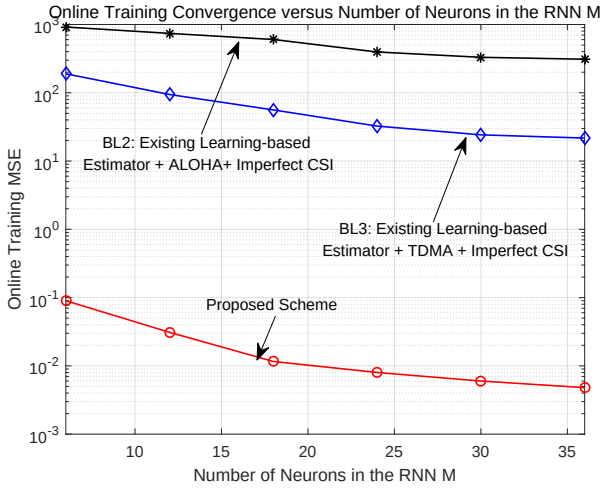


(b) Online training MSE versus the number of neurons $M$.

Figure 9. Illustration of state estimation and online training performance versus sensor training pilot length $L$. The system parameters are configured as follows: the online training parameter $\bar{\eta} = 0.045\mathbf{I}_{6\times 1}$, $\eta = 0.045$, the sensor transmission probability $\mathbb{E}\left[\delta_i\left(k\right)\right] = 0.2$, the number of sensors $N = 6$, the sensor training pilot length $L = 36$, and the sensor transmission SNR $\rho = 10$ dB.

## VI. Conclusion

In this paper, we consider AI-based remote state estimation for nonlinear systems with unknown plant dynamics and non-invertible nonlinear observations. Utilizing a state diffeomorphism, the original system is transformed into a canonical form with a linear rank deficient observation matrix. We propose a novel RNN remote state estimator based on the pole placement design associated with the transformed rank deficient state

measurement matrices. We further propose a novel online training algorithm such that the RNN at the remote estimator can effectively learn the unknown nonlinear plant dynamics. Compared with the existing learning based remote estimators, the proposed scheme not only effectively addresses the divergence issue over wireless networks but also exploits the non-invertible nonlinear state observations and the imperfect CSI to further enhance the estimation performance. Moreover, the proposed scheme achieves almost sure estimation stability and online training convergence in the high SNR regime.

## APPENDIX

### A. Proof Theorem 1

Since $\mathbb{E}\left[h_i\left(k\right)\right]=0$, it follows that

$$\mathbb{E}\left[y_{k+1}-\sum_{i=1}^{N}\sqrt{\rho}h_i\left(k+1\right)q_i\left(\bar{\mathbf{x}}_{k+1}\right)\right]=0. \tag{43}$$

As such, taking the expectation on both sides of (13), it follows that

$$\mathbb{E}\left[\overline{\mathbf{W}}_k\right]=\overline{\mathbf{W}}_0. \tag{44}$$

Note that $\left\|\cdot\right\|^2$ is a convex operator, it follows that $\forall k\in\mathbb{N}^+$, the following inequality holds:

$$\mathbb{E}\left[\left\|\overline{\mathbf{W}}_k-\mathbf{W}\right\|_F^2\right]\geq\left\|\mathbb{E}\left[\overline{\mathbf{W}}_k-\mathbf{W}\right]\right\|_F^2=\left\|\overline{\mathbf{W}}_0-\overline{\mathbf{W}}\right\|_F^2. \tag{45}$$

As a result, Theorem 1 is proved.

### B. Proof of Lemma 1 and Lemma 2

Note that the mapping $\mathbf{\Psi}\left(\cdot\right)$ is constructed as $\mathbf{z}_k=\mathbf{\Psi}\left(\mathbf{x}_k\right)=\left[\begin{array}{c}\mathbf{q}\left(\mathbf{x}_k\right)\\\mathbf{x}_k\end{array}\right]$. As a result, $\mathbf{x}_k$ can be obtained from $\mathbf{z}_k$ as:

$$\mathbf{x}_k=\mathbf{\Gamma}\mathbf{z}_k, \tag{46}$$

where $\mathbf{\Gamma}$ is given by (15). Therefore, $\mathbf{\Psi}\left(\cdot\right)$ is invertible and $\mathbf{\Psi}^{-1}\left(\mathbf{z}_k\right)=\mathbf{\Gamma}\mathbf{z}_k$.

Note that $\mathbf{x}_k=\mathbf{\Psi}^{-1}\left(\mathbf{z}_k\right)$, it follows that the nonlinear plant dynamics $\mathbf{x}_{k+1}=\mathbf{f}\left(\mathbf{x}_k\right)$ is equivalent to

$$\mathbf{z}_{k+1}=\mathbf{\Psi}\left(\mathbf{f}\left(\mathbf{\Psi}^{-1}\left(\mathbf{z}_k\right)\right)\right). \tag{47}$$

Further note that the received signal model (4) can be represented as:

$$\begin{aligned}y_k&=\mathbf{h}_k\left[\begin{array}{c}\mathbf{q}\left(\mathbf{x}_k\right)\\\mathbf{0}_{S\times1}\end{array}\right]+v_k\\&=\mathbf{h}_k\mathbf{z}_k+v_k,\end{aligned} \tag{48}$$

and it follows that Lemma 1 is proved.

Note that $\mathbb{E}\left[h_i\left(k\right)h_j\left(k\right)\right]=0,\forall i\neq j$, and $\mathbb{E}\left[h_i^2\left(k\right)\right]=1$, it follows that

$$\mathbb{E}\left[\left(\sum_{i=1}^{N}h_i\left(k\right)\right)\mathbf{h}_k\mathbf{z}_k\right]=\sum_{i=1}^{N}q_i\left(\mathbf{x}_k\right). \tag{49}$$

Similarly, we have

$$\begin{aligned}&\mathbb{E}\left[\left(\sum_{i=1}^{N}h_i\left(k\right)\right)\mathbf{h}_k\mathbf{\Psi}\left(\mathbf{f}\left(\mathbf{\Psi}^{-1}\left(\mathbf{z}_k\right)\right)\right)\right]\\&=\mathbb{E}\left[\left(\sum_{i=1}^{N}h_i\left(k\right)\right)\mathbf{h}_k\mathbf{\Psi}\left(\mathbf{f}\left(\mathbf{x}_k\right)\right)\right]\\&=q\left(\mathbf{f}\left(\mathbf{x}_k\right)\right);\end{aligned} \tag{50}$$

and

$$\begin{aligned}&\mathbb{E}\left[\left(\sum_{i=1}^{N}h_i\left(k\right)\right)\mathbf{h}_k\left(\mathbf{\Psi}\circ\mathbf{f}\circ\mathbf{\Psi}^{-1}\right)^{S-1}\left(\mathbf{z}_k\right)\right]\\&=q\left(\mathbf{f}^{(S-1)}\left(\mathbf{x}_k\right)\right).\end{aligned} \tag{51}$$

Therefore, we conclude that:

$$\widetilde{\mathbf{\Phi}}\left(\mathbf{z}_k\right)=\mathbf{\Phi}\left(\mathbf{x}_k\right). \tag{52}$$

Since mapping $\mathbf{\Phi}\left(\cdot\right):\mathbb{R}^{S\times1}\rightarrow\mathbb{R}^{S\times1}$ is a diffeomorphism, it follows that the mapping $\widetilde{\mathbf{\Phi}}\left(\cdot\right):\mathbb{R}^{(N+S)\times1}\rightarrow\mathbb{R}^{S\times1}$ in (18) is also a diffeomorphism. As a result, Lemma 2 is proved.

### C. Proof of Lemma 3

Denote the state estimation error of the proposed RNN-based state estimator (26) as $\mathbf{e}_k=\mathbf{z}_k-\hat{\mathbf{z}}_k$. Denote the weight error of the proposed RNN training algorithm (33) as $\tilde{\mathbf{W}}_k=\mathbf{W}-\hat{\mathbf{W}}_k$. Based on the proposed RNN based state estimator (26) and the nonlinear system parameterization (25), it follows that the state estimation error has the following dynamics:

$$\begin{aligned}\mathbf{e}_{k+1}&=\mathbf{U}\mathbf{W}\varphi\left(\mathbf{z}_k\right)+\mathbf{U}\epsilon\left(\mathbf{z}_k\right)-\mathbf{U}\hat{\mathbf{W}}_k\varphi\left(\hat{\mathbf{z}}_k\right)\\&=\mathbf{U}\mathbf{W}\left(\varphi\left(\mathbf{z}_k\right)-\varphi\left(\hat{\mathbf{z}}_k\right)\right)+\mathbf{U}\tilde{\mathbf{W}}_k\varphi\left(\hat{\mathbf{z}}_k\right)+\mathbf{U}\epsilon\left(\mathbf{z}_k\right).\end{aligned} \tag{53}$$

Therefore, the term $\mathbf{e}_{k+1}^T\mathbf{P}\mathbf{e}_{k+1}$ satisfies:

$$\begin{aligned}\mathbf{e}_{k+1}^T\mathbf{P}\mathbf{e}_{k+1}=&\left\|\mathbf{P}^{\frac{1}{2}}\mathbf{U}\left(\mathbf{W}\left(\varphi\left(\mathbf{z}_k\right)-\varphi\left(\hat{\mathbf{z}}_k\right)\right)+\epsilon\left(\mathbf{z}_k\right)\right)\right\|_F^2+\\&2\varphi^T\left(\hat{\mathbf{z}}_k\right)\left(\mathbf{W}-\hat{\mathbf{W}}_k\right)^T\mathbf{U}^T\mathbf{P}\mathbf{U}\left(\mathbf{W}\left(\varphi\left(\mathbf{z}_k\right)-\varphi\left(\hat{\mathbf{z}}_k\right)\right)+\epsilon\left(\mathbf{z}_k\right)\right)\\&+\left\|\mathbf{P}^{\frac{1}{2}}\mathbf{U}\left(\mathbf{W}-\hat{\mathbf{W}}_k\right)\varphi\left(\hat{\mathbf{z}}_k\right)\right\|_F^2.\end{aligned} \tag{54}$$

Similarly, based on the proposed RNN training algorithm (33) and noting that $\hat{\mathbf{h}}_k=\mathbf{h}_k+\frac{1}{L}\mathbf{v}_k^L\mathbf{L}$, the weight error $\tilde{\mathbf{W}}_k$ has the following dynamics:

$$\begin{aligned}&\tilde{\mathbf{W}}_{k+1}=\\&\tilde{\mathbf{W}}_k-\eta\rho^{-1}\mathbf{U}^T\mathbf{P}\mathbf{U}\left(\hat{\mathbf{h}}_k^T\left(y_{k+1}-\hat{\mathbf{h}}_k\hat{\mathbf{z}}_{k+1}\right)\right)^T\varphi^T\left(\hat{\mathbf{z}}_k\right)\\&=\tilde{\mathbf{W}}_k-\eta\rho^{-1}\mathbf{U}^T\mathbf{P}\mathbf{U}\Bigg(\hat{\mathbf{h}}_k^T\left(\left(\hat{\mathbf{h}}_k^T-\frac{1}{L}\mathbf{v}_k^L\mathbf{L}\right)\mathbf{z}_{k+1}\right.\\&\left.-\hat{\mathbf{h}}_k\hat{\mathbf{z}}_{k+1}+v_k\right)\varphi^T\left(\hat{\mathbf{z}}_k\right)\\&=\tilde{\mathbf{W}}_k-\eta\rho^{-1}\mathbf{U}^T\mathbf{P}\mathbf{U}\left(\hat{\mathbf{h}}_k^T\hat{\mathbf{h}}_k\mathbf{e}_{k+1}\right)\varphi^T\left(\hat{\mathbf{z}}_k\right)\\&+\eta\rho^{-1}\mathbf{U}^T\mathbf{P}\mathbf{U}\left(\hat{\mathbf{h}}_k^T\frac{1}{L}\mathbf{v}_k^L\mathbf{L}\mathbf{z}_{k+1}-v_k\right)\varphi^T\left(\hat{\mathbf{z}}_k\right).\end{aligned} \tag{55}$$

As such, the term $\mathbb{E}\left[\frac{1}{\eta}\left\|\mathbf{W}-\hat{\mathbf{W}}_k\right\|_F^2\right]$ obeys:

$$\mathbb{E}\left[\frac{1}{\eta}\left\|\mathbf{W}-\hat{\mathbf{W}}_{k+1}\right\|_F^2\right]\leq$$
$$\mathbb{E}\left[\frac{1}{\eta}\left\|\mathbf{W}-\hat{\mathbf{W}}_{k}\right\|_F^2\right]+2\varphi^T\left(\hat{\mathbf{z}}_k\right)\left(\mathbf{W}-\hat{\mathbf{W}}_k\right)^T\mathbf{U}^T\mathbf{P}\mathbf{U}$$
$$\cdot\left(\rho^{-1}\left(\hat{\mathbf{h}}_k^T\mathbf{h}_k+\frac{1}{L}\hat{\mathbf{h}}_k^T\mathbf{v}_k^L\mathbf{L}\right)\hat{\mathbf{e}}_{k+1}-\frac{1}{\rho L}\hat{\mathbf{h}}_k^T\mathbf{v}_k^L\mathbf{L}\mathbf{x}_{k+1}\right)$$
$$+\eta\left\|\left(\rho^{-1}\left(\hat{\mathbf{h}}_k^T\mathbf{h}_k+\frac{1}{L}\hat{\mathbf{h}}_k^T\mathbf{v}_k^L\mathbf{L}\right)\hat{\mathbf{e}}_{k+1}-\frac{1}{\rho L}\hat{\mathbf{h}}_k^T\mathbf{v}_k^L\mathbf{L}\mathbf{x}_{k+1}\right)\right\|_F^2$$
$$+\eta\left\|\rho^{-1}\mathbf{P}^{\frac{1}{2}}\mathbf{U}\hat{\mathbf{h}}_k^T v_{k+1}\varphi^T\left(\hat{\mathbf{z}}_k\right)\right\|_F^2. \tag{56}$$

Substitute (54) and (56) into (34), it follows inequality (36). Therefore, Lemma 3 is proved.

### *D. Proof of Theorem 2 and Theorem 3*

Based on (54) and (56), it follows that

$$\mathbf{e}_{k+1}^T\mathbf{P}\mathbf{e}_{k+1}+\mathbb{E}\left[\frac{1}{\eta}\left\|\mathbf{W}-\hat{\mathbf{W}}_{k+1}\right\|_F^2\right]$$
$$\leq 2\left(\|\mathbf{W}\varphi\|+\frac{1}{\sqrt{\rho L}}\right)\left\|\sum_{i=0}^{\infty}\left(\left(\tilde{\mathbf{\Pi}}\right)^i\right)^T\left(\tilde{\mathbf{\Pi}}\right)^i\right\|\mathbf{e}_k^T\mathbf{e}_k$$
$$+\frac{\eta\left(S+N\right)}{\rho}\left\|\sum_{i=0}^{\infty}\left(\left(\tilde{\mathbf{\Pi}}\right)^i\right)^T\left(\tilde{\mathbf{\Pi}}\right)^i\right\|^2+\left(\epsilon_M^2+\frac{\alpha}{\rho L}\right)$$
$$\cdot 2\left\|\sum_{i=0}^{\infty}\left(\left(\tilde{\mathbf{\Pi}}\right)^i\right)^T\left(\tilde{\mathbf{\Pi}}\right)^i\right\|+\eta\left\|\sum_{i=0}^{\infty}\left(\left(\tilde{\mathbf{\Pi}}\right)^i\right)^T\left(\tilde{\mathbf{\Pi}}\right)^i\right\|^2\mathbf{e}_k^T\mathbf{e}_k$$
$$+\mathbf{e}_{k+1}^T\left(\tilde{\mathbf{\Pi}}\right)^T\mathbf{P}\tilde{\mathbf{\Pi}}\mathbf{e}_{k+1}+\mathbb{E}\left[\frac{1}{\eta}\left\|\mathbf{W}-\hat{\mathbf{W}}_{k}\right\|_F^2\right]. \tag{57}$$

As a result,

$$\left\|\mathbf{e}_{k+1}\right\|_F^2-\left\|\mathbf{e}_k\right\|_F^2+\mathbb{E}\left[\frac{1}{\eta}(\left\|\mathbf{W}-\hat{\mathbf{W}}_{k+1}\right\|_F^2-\left\|\mathbf{W}-\hat{\mathbf{W}}_{k}\right\|_F^2)\right]$$
$$\leq\left(2\left(\|\mathbf{W}\varphi\|+\frac{1}{\sqrt{\rho L}}\right)\left\|\sum_{i=0}^{\infty}\left(\left(\tilde{\mathbf{\Pi}}\right)^i\right)^T\left(\tilde{\mathbf{\Pi}}\right)^i\right\|+\eta\right.$$
$$\cdot\left\|\sum_{i=0}^{\infty}\left(\left(\tilde{\mathbf{\Pi}}\right)^i\right)^T\left(\tilde{\mathbf{\Pi}}\right)^i\right\|^2-1\Bigg)\left\|\mathbf{e}_k\right\|_F^2+\frac{\eta\left(S+N\right)}{\rho}$$
$$\cdot\left\|\sum_{i=0}^{\infty}\left(\left(\tilde{\mathbf{\Pi}}\right)^i\right)^T\left(\tilde{\mathbf{\Pi}}\right)^i\right\|^2+2\left(\epsilon_M^2+\frac{\alpha}{\rho L}\right)$$
$$\cdot\left\|\sum_{i=0}^{\infty}\left(\left(\tilde{\mathbf{\Pi}}\right)^i\right)^T\left(\tilde{\mathbf{\Pi}}\right)^i\right\|. \tag{58}$$

Based on (58), a sufficient condition for negative drift is that $(2(\|\mathbf{W}\varphi\|+\frac{1}{\sqrt{\rho L}}))\|\sum_{i=0}^{\infty}\left(\left(\tilde{\mathbf{\Pi}}\right)^i\right)^T\left(\tilde{\mathbf{\Pi}}\right)^i\|+\eta\|\sum_{i=0}^{\infty}\left(\left(\tilde{\mathbf{\Pi}}\right)^i\right)^T\left(\tilde{\mathbf{\Pi}}\right)^i\|^2-1<0$, which leads to the Inequality (37). Therefore, if the sufficient condition (37) for stability in Theorem 2 is satisfied, both the state estimation and the RNN online training are stable. Therefore, Theorem 2 is proved.

Summing the above inequality (58) of both sides from $k=1$ to $k=T$, it follows that

$$\left\|\mathbf{e}_{T+1}\right\|_F^2-\left\|\mathbf{e}_1\right\|_F^2+\mathbb{E}\left[\frac{1}{\eta}(\left\|\mathbf{W}-\hat{\mathbf{W}}_{T+1}\right\|_F^2-\left\|\mathbf{W}-\hat{\mathbf{W}}_{1}\right\|_F^2)\right]$$
$$\leq\left(2\left(\|\mathbf{W}\varphi\|+\frac{1}{\sqrt{\rho L}}\right)\left\|\sum_{i=0}^{\infty}\left(\left(\tilde{\mathbf{\Pi}}\right)^i\right)^T\left(\tilde{\mathbf{\Pi}}\right)^i\right\|+\eta\right.$$
$$\cdot\left\|\sum_{i=0}^{\infty}\left(\left(\tilde{\mathbf{\Pi}}\right)^i\right)^T\left(\tilde{\mathbf{\Pi}}\right)^i\right\|^2-1\Bigg)\sum_{k=1}^{T}\left\|\mathbf{e}_k\right\|_F^2+\frac{T\eta\left(S+N\right)}{\rho}$$
$$\cdot\left\|\sum_{i=0}^{\infty}\left(\left(\tilde{\mathbf{\Pi}}\right)^i\right)^T\left(\tilde{\mathbf{\Pi}}\right)^i\right\|^2+2T\left(\epsilon_M^2+\frac{\alpha}{\rho L}\right)$$
$$\cdot\left\|\sum_{i=0}^{\infty}\left(\left(\tilde{\mathbf{\Pi}}\right)^i\right)^T\left(\tilde{\mathbf{\Pi}}\right)^i\right\|. \tag{59}$$

Arranging $(2(\|\mathbf{W}\varphi\|+\frac{1}{\sqrt{\rho L}}))\|\sum_{i=0}^{\infty}\left(\left(\tilde{\mathbf{\Pi}}\right)^i\right)^T\left(\tilde{\mathbf{\Pi}}\right)^i\|+\eta\|\sum_{i=0}^{\infty}\left(\left(\tilde{\mathbf{\Pi}}\right)^i\right)^T\left(\tilde{\mathbf{\Pi}}\right)^i\|^2-1)\sum_{k=1}^{T}\left\|\mathbf{e}_k\right\|_F^2$ to the L.H.S. of (59), neglecting the non-negative terms $\frac{1}{\eta}\left\|\mathbf{W}-\hat{\mathbf{W}}_{T+1}\right\|_F^2$ and $\left\|\mathbf{e}_{T+1}\right\|_F^2$, and dividing both sides of (59) by $(2(\|\mathbf{W}\varphi\|+\frac{1}{\sqrt{\rho L}})\|\sum_{i=0}^{\infty}\left(\left(\tilde{\mathbf{\Pi}}\right)^i\right)^T\left(\tilde{\mathbf{\Pi}}\right)^i\|+\eta\|\sum_{i=0}^{\infty}\left(\left(\tilde{\mathbf{\Pi}}\right)^i\right)^T\left(\tilde{\mathbf{\Pi}}\right)^i\|^2-1)T$, it follows:

$$\frac{1}{T}\sum_{k=1}^{T}\mathbb{E}\left[\left\|\mathbf{x}_k-\hat{\mathbf{x}}_k\right\|^2\right]<\left(2\left\|\sum_{i=0}^{\infty}\left(\left(\tilde{\mathbf{\Pi}}\right)^i\right)^T\left(\tilde{\mathbf{\Pi}}\right)^i\right\|\right.$$
$$\cdot\left(\epsilon_M^2+\frac{\alpha}{\rho L}\right)+\frac{\eta\left(S+N\right)}{\rho}\left\|\sum_{i=0}^{\infty}\left(\left(\tilde{\mathbf{\Pi}}\right)^i\right)^T\left(\tilde{\mathbf{\Pi}}\right)^i\right\|^2\Bigg)$$
$$\cdot\left(1-2\left(\|\mathbf{W}\varphi\|+\frac{1}{\sqrt{\rho L}}\right)\left\|\sum_{i=0}^{\infty}\left(\left(\tilde{\mathbf{\Pi}}\right)^i\right)^T\left(\tilde{\mathbf{\Pi}}\right)^i\right\|\right.$$
$$\left.-\eta\left\|\sum_{i=0}^{\infty}\left(\left(\tilde{\mathbf{\Pi}}\right)^i\right)^T\left(\tilde{\mathbf{\Pi}}\right)^i\right\|^2\right)^{-1}+\frac{1}{T}\left(\left\|\mathbf{e}_1\right\|_F^2+\frac{1}{\eta}\left\|\mathbf{W}-\hat{\mathbf{W}}_1\right\|_F^2\right). \tag{60}$$

Taking the limit of $T$ on both sides of (60), and note that $\limsup_{T\to\infty}\frac{1}{T}(\|\mathbf{e}_1\|_F^2+\frac{1}{\eta}\left\|\mathbf{W}-\hat{\mathbf{W}}_1\right\|_F^2)=0$, it follows inequality (38).

Based on Equality (53), it follows that

$$\left\|\mathbf{e}_{k+1}\right\|\geq\left\|\mathbf{W}\varphi\left(\mathbf{z}_k\right)-\hat{\mathbf{W}}_k\varphi\left(\mathbf{z}_k\right)\right\|-\left\|\mathbf{W}\varphi\right\|\left\|\mathbf{e}_k\right\|-\epsilon_M. \tag{61}$$

As a result,

$$\left\|\mathbf{W}\varphi\left(\mathbf{z}_k\right)-\hat{\mathbf{W}}_k\varphi\left(\mathbf{z}_k\right)\right\|_F^2\leq 3\epsilon_M^2+3\left\|\mathbf{W}\varphi\right\|^2\left\|\mathbf{e}_k\right\|^2$$
$$+3\left\|\mathbf{e}_{k+1}\right\|^2. \tag{62}$$

Summing the above inequality (62) of both sides from $k=1$ to $k=T$, and taking the expectation and dividing both sides by $T$, it follows:

$$\frac{1}{T}\sum_{k=1}^{T}\mathbb{E}\left[\left\|\mathbf{W}\varphi\left(\mathbf{z}_k\right)-\hat{\mathbf{W}}_k\varphi\left(\mathbf{z}_k\right)\right\|^2\right]\leq 3\epsilon_M^2+ \\ +\frac{1}{T}\sum_{k=1}^{T}\mathbb{E}\left[3\left\|\mathbf{W}\varphi\right\|^2\left\|\mathbf{e}_k\right\|^2+3\left\|\mathbf{e}_{k+1}\right\|^2\right]. \quad (63)$$

Taking the limit of $T$ on both sides of (63), and note that $\limsup_{T\to\infty}\frac{1}{T}\sum_{k=1}^{T}\mathbb{E}\left[\left\|\mathbf{e}_k\right\|^2\right]=\limsup_{T\to\infty}\frac{1}{T}\sum_{k=1}^{T}\mathbb{E}\left[\left\|\mathbf{e}_{k+1}\right\|^2\right]$, it follows inequality (39). Therefore, Theorem 3 is proved.

### *E. Proof of Corollary 1*

Note that NN approximation error $\epsilon\left(\mathbf{z}_k\right)$ vanishes as the number of neurons $M$ approaches infinity, i.e.,

$$\lim_{M\to\infty}\left\|\epsilon\left(\mathbf{z}_k\right)\right\|_F^2\leq\lim_{M\to\infty}\left\|\epsilon_M\right\|_F^2\leq 0. \quad (64)$$

As a result,

$$\lim_{\rho\to\infty}\lim_{M\to\infty}\lim_{L\to\infty}\left(\left\|\mathbf{W}\varphi\right\|+\frac{1}{\sqrt{\rho L}}\right)=\left\|\mathbf{\Psi}\circ\mathbf{f}\circ\left(\mathbf{\Psi}^{-1}\right)\right\|. \quad (65)$$

Therefore, when $\rho$, $M$ and $L$ all approach infinity, the sufficient condition (37) in Theorem 2 reduces to condition (40) in Corollary 1.

Moreover, under condition (40), taking the limit w.r.t. $\rho$, $M$ and $L$ on both side of 38, it follows that

$$\lim_{\rho\to\infty}\lim_{M\to\infty}\lim_{L\to\infty}\limsup_{T\to\infty}\frac{1}{T}\sum_{k=1}^{T}\mathbb{E}[||\mathbf{x}_k-\hat{\mathbf{x}}_k||^2]\leq 0. \quad (66)$$

Since $(\mathbf{x}_k-\hat{\mathbf{x}}_k)$ is Markovian, it follows that:

$$\lim_{\rho\to\infty}\lim_{M\to\infty}\lim_{L\to\infty}\limsup_{k\in\mathbb{N}^+}\mathbb{E}\left[\left\|\mathbf{x}_k-\hat{\mathbf{x}}_k\right\|_2^2\right]=0. \quad (67)$$

As a result, Equation (41) holds.

Similarly, under condition (40), taking the limit w.r.t. $\rho$, $M$ and $L$ on both side of 39 and note that:

$$\lim_{M\to\infty}\mathbf{W}\varphi\left(\mathbf{z}_k\right)=\mathbf{\Psi}\left(\mathbf{f}\left(\mathbf{\Psi}^{-1}\left(\mathbf{z}_k\right)\right)\right), \quad (68)$$

it follows that

$$\lim_{\rho\to\infty}\lim_{M\to\infty}\lim_{L\to\infty}\limsup_{T\to\infty}\frac{1}{T} \\ \sum_{k=1}^{T}\mathbb{E}\left[\left\|\mathbf{\Psi}\left(\mathbf{f}\left(\mathbf{\Psi}^{-1}\left(\mathbf{z}_k\right)\right)\right)-\hat{\mathbf{W}}_k\varphi\left(\mathbf{z}_k\right)\right\|^2\right]\leq 0. \quad (69)$$

Therefore,

$$\lim_{\rho\to\infty}\lim_{M\to\infty}\lim_{L\to\infty}\limsup_{k\in\mathbb{N}^+}\mathbb{E}[||\mathbf{\Psi}\left(\mathbf{f}\left(\mathbf{\Psi}^{-1}\left(\mathbf{z}_k\right)\right)\right) \\ -\hat{\mathbf{W}}_k\varphi\left(\mathbf{z}_k\right)||^2]=0, \quad (70)$$

and Equation (42) holds. Therefore, Corollary 1 is proved.

## REFERENCES


[1] P. Schulz, M. Matthe, and H. Klessig et al., "Latency critical IoT applications in 5G: Perspective on the design of radio interface and network architecture," *IEEE Commun. Mag.*, vol. 55, no. 2, pp. 70-78, 2017.

[2] A. Zanella, N. Bui, A. Castellani, L. Vangelista, and M. Zorzi, "Internet of things for smart cities," *IEEE Internet of Things Journal*, vol. 1, no. 1, pp. 22-32, 2014.

[3] L. Schenato, B. Sinopoli, M. Franceschetti, K. Poolla and S. Sastry, "Foundations of control and estimation over lossy networks," *Proc. IEEE*, vol. 95, no. 1, pp. 163-187, 2007.

[4] B. Sinopoli, L. Schenato, M. Franceschetti, K. Poolla, M. Jordan, and S. S. Sastry, "Kalman filtering with intermittent observations," *IEEE Trans. Autom. Control*, vol. 49, no. 9, pp. 1453-1464, 2004.

[5] X. Dong, B. Yu, Z. Shi, and Y. Zhong, "Time-varying formation control for unmanned aerial vehicles: Theories and applications," *IEEE Trans. Control Syst. Technol.*, vol. 23, no. 1, pp. 340–348, Jan. 2015.

[6] V. C. Gungor, G. P. Hancke, "Industrial wireless sensor networks: Challenges, design principles, and technical approaches," *IEEE Trans. Ind. Electron.*, vol. 56, no. 10, pp. 4258-4265, 2009.

[7] S. Cai, V. Lau, "Modulation-Free M2M communications for mission-critical M2M applications," *IEEE Trans. Signal and Info. Process. Networks*, vol. 4, no. 2, pp.248-263, 2018.

[8] X. Liu and A. Goldsmith, "Kalman filtering with partial observation losses," in *Proc. IEEE Conf. Decision Contr.*, Bahamas, Dec. 2004, vol. 4, pp. 4180–4186.

[9] S. Deshmukh, B. Natarajan and A. Pahwa, "State estimation over a lossy network in spatially distributed cyber-physical systems," *IEEE Trans. Signal Process.*, vol. 62, no. 15, pp. 3911-3923, 2014.

[10] C. Y. Lu, "A delay-range-dependent approach to design state estimator for discrete-time recurrent neural networks with interval time-varying delay," *IEEE Trans. Circuits Syst. II, Exp. Briefs*, vol. 55, no. 11, pp. 1163-1167, 2008.

[11] H. Huang and G. Feng, "A scaling parameter approach to delaydependent state estimation of delayed neural networks," *IEEE Trans. Circuits Syst. II, Exp. Briefs*, vol. 57, no. 1, pp. 36-40, Jan. 2010

[12] M. Liu and H. Chen, "H∞ state estimation for discrete-time delayed systems of the neural network type with multiple missing measurements," *IEEE Trans. Neural Netw. Learn. Syst.*, vol. 26, no. 12, pp. 2987-2998, Dec. 2015.

[13] S. Yu, K. Emami, T. Fernando, H. H.-C. Iu, and K. P. Wong, "State estimation of doubly fed induction generator wind turbine in complex power systems," *IEEE Trans. Power Syst.*, vol. 31, no. 6, pp. 4935-4944, 2016.

[14] S. Ibrir, "LPV approach to continuous and discrete nonlinear observer design," in *Proc. IEEE Conf. Decision Contr.*, 2009, pp. 8206–8211.

[15] D. Noh, N. H. Jo, and J. H. Seo, "Nonlinear observer design by dynamic observer error linearization," *IEEE Trans. Autom. Contr.*, vol. 49, no. 10, pp. 1746-1750, 2004.

[16] M. K. Al-Sharman, Y. Zweiri, M. A. K. Jaradat, R. Al-Husari, D. Gan, and L. D. Seneviratne, "Deep-learning-based neural network training for state estimation enhancement: Application to attitude estimation," *IEEE Trans. Instrum. Meas.*, vol. 69, no. 1, pp. 24-34, 2020.

[17] Y. H. Kim, F. L. Lewis, and C. T. Abdallah, "A dynamic recurrent neural-network-based adaptive observer for a class of nonlinear systems," *Automatica*, vol. 33, no. 8, pp. 1539-1543, 1997.

[18] Y. H. Kim, F. L. Lewis, and C. T. Abdallah, "Nonlinear observer design using dynamic recurrent neural networks," in *Proc. IEEE Conf. Decision Contr.*, 1996, pp. 949–954

[19] S. N. Huang, K. K. Tan, T .H. Lee, "Further result on a dynamic recurrent neural-network-based adaptive observer for a class of nonlinear systems," *Automatica*, vol. 41, no. 12, pp. 2161-2162, 2005.

[20] C. Hua, C. Yu, X. Guan, "Neural network observer-based networked control for a class of nonlinear systems," *Neurocomput.*, vol. 133, pp. 103-110, 2014.

[21] A. Y. Alanis, E. N. Sanchez, A. G. Loukianov, and M. A. Perez, "Realtime recurrent neural state estimation," *IEEE Trans. Neural Netw.*, vol. 22, no. 3, pp. 497–505, 2011.

[22] A. Y. Alanis, E. N. Sanchez, A. G. Loukianov, and M. A. Perez-Cisneros, "Real-time discrete neural block control using sliding modes for electric induction motors," *IEEE Trans. Control Syst. Technol.*, vol. 18, no. 1, pp. 11–21, 2010.

[23] M. D. Mora, A. Germani, and C. Manes, "Design of state observers from a drift-observability property," *IEEE Trans. Automat. Contr.*, vol. 45, pp. 1536 -1540, 2000.

[24] S. S. Alam and B. Natarajan, "Stability of agent based distributed model predictive control over a lossy network." *IEEE Trans. Signal and Inf. Process. over Networks*, vol. 1, no. 4, pp. 235-246, 2015.
[25] D. Barcelli and A. Bemporad, "Decentralized model predictive control of dynamically-coupled linear systems: Tracking under packet loss," *IFAC Proceedings Volumes*, vol. 42, no. 20, pp. 204-209, 2009.
[26] U. A. Khan, J. M. Moura, "Distributing the Kalman filter for large-scale systems," *IEEE Trans. Signal Process.*, vol. 56, no. 10, pp: 4919-4935, 2008.
[27] S. S. Alam, B. Natarajan, A. Pahwa, and S. Curto, "Agent based state estimation in smart distribution grid," *IEEE Latin America Trans.*, vol. 13, no. 2, pp.496-502, 2015..
[28] H. Kantz and T. Schreiber, *Nonlinear Time Series Analysis*. Cambridge, U.K.: Cambridge Univ. Press, 1997.
[29] A. I. Mees, Ed., *Nonlinear Dynamics and Statistics*, Boston: Birkhauser, 2001.
[30] M. J. Neely, "Stochastic network optimization with application to communication and queueing systems," *Synthesis Lectures on Communication Networks*, vol. 3, no. 1, pp. 1-211, 2010.
[31] L. Huang and M. J. Neely, "Utility optimal scheduling in energy harvesting networks," *IEEE/ACM Trans. Networking*, vol. 21, no. 4, pp. 1117-1130, Aug. 2013.
[32] Y. Cui, V. K. N. Lau, R. Wang, H. Huang, and S. Zhang, "A survey on delay-aware resource control for wireless systems—Large deviation theory, stochastic Lyapunov drift and distributed stochastic Learning," *IEEE Trans. Inf. Theory*, vol. 58, no. 3, pp. 1677-1701, Mar. 2012.
[33] M. J. Neely, E.Modiano and C. E. Rohrs, "Dynamic power allocation and routing for time-varying wireless networks," *IEEE J. Sel. Areas Commun.*, vol. 23, no. 1, pp. 89-103, 2005.
[34] S. Cai, V. Lau, "Modulation-Free M2M communications for mission-critical M2M applications," *IEEE Trans. Signal and Inf. Process. over Networks*, vol. 4, no. 2, pp. 248-263, 2017.
[35] L. Dai, "Toward a coherent theory of CSMA and Aloha," *IEEE Trans.Wireless Commun.*, vol. 12, no. 7, pp. 3428 - 3444, Jul. 2013.
[36] Y. Liu, C. Yuen, X. Cao, N. U. Hassan, and J. Chen, "Design of a scalable hybrid MAC protocol for heterogeneous M2M networks," *IEEE Internet of Things Journal*, vol. 1, no. 1, pp. 99-111, Mar. 2014.